Sistemi di Supervisione Adattativi

Parte 4

Silvio Simani

September 2018

URL: http://www.silviosimani.it/lessons42.html

E-mail: silvio.simani@unife.it

Lecture Main Topics

- General introduction
  - State-of-the-art review
  - Fault diagnosis nomenclature
- Main methods for fault diagnosis
  - Parameter estimation methods
  - Observer and filter approaches
  - Parity relations
  - Neural networks and fuzzy systems
- **Application examples**
- Concluding remarks

Application Examples

- Simulated case studies
- Identification/FDI applications
- Real processes
- Research works
- Undergraduate theses topics

Simulated Application Examples

Simulated Gas Turbine

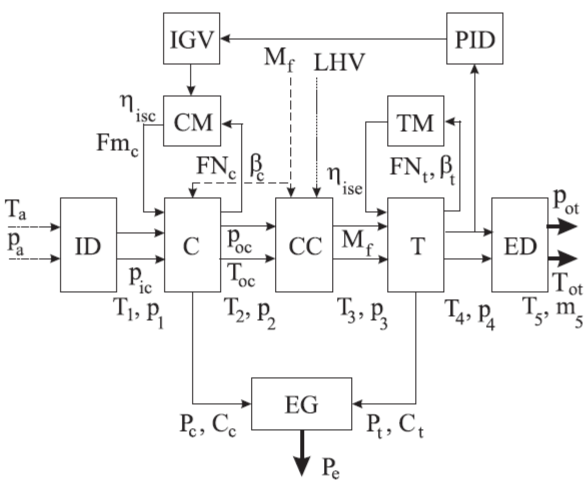

C	Compressor
CC	Combustor (Combustion Chamber)
CM	Compressor Map
ED	Exhaust Duct
EG	Electric Generator
ID	Intake Duct
IGV	Inlet Guide Vanes
PID	Proportional Integral Derivative Controller
T	Turbine
TM	Turbine Map

Figure 5.2: Block diagram of the single–shaft gas turbine.

Simulated Application Examples (Cont'd)

Simulated Gas Turbine

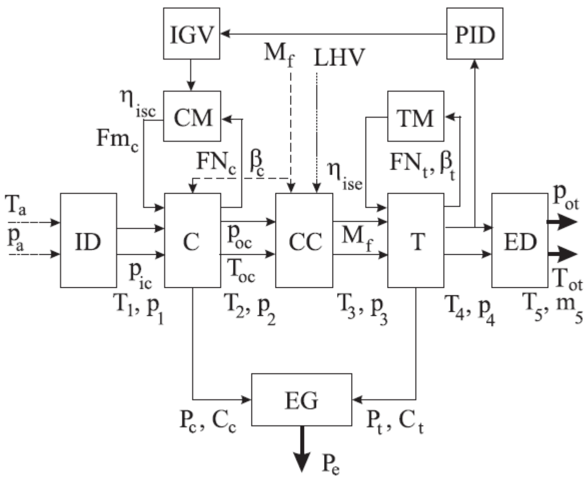

Figure 5.2: Block diagram of the single–shaft gas turbine.

M_f	Fuel mass flow rate
LHV	Lower Heating Value
η_{isc}	Isentropic compressor efficiency
Fm_c	Compressor mass flow function
FN_c	Compressor rotational speed function
β_c	Compressor pressure ratio
η_{ise}	Isentropic expansion efficiency
FN_t	Turbine rotational speed function
β_t	Turbine pressure ratio
T_i	i–th section (module) temperature ($i = 1, \cdots, 5$)
p_i	i–th section (module) pressure ($i = 1, \cdots, 5$)
m_5	5–th module mass flow rate
T_a	Ambient temperature
p_a	Ambient pressure
P_c	Compressor power
P_t	Turbine power
C_c	Compressor torque
C_t	Turbine torque
P_e	Electrical power

Simulated Application Examples (Cont'd)

Simulated Gas Turbine

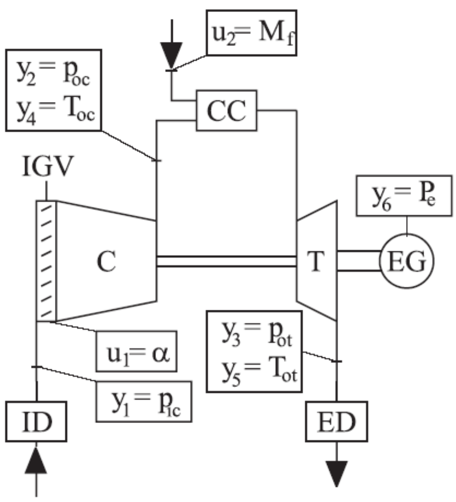

$u_1(t)$, Inlet Guide Vane (IGV) angular position (α);

$u_2(t)$, fuel mass flow rate (M_f).

$y_1(t)$, pressure at the compressor inlet (p_{ic});

$y_2(t)$, pressure at the compressor outlet (p_{oc});

$y_3(t)$, pressure at the turbine outlet (p_{ot});

$y_4(t)$, temperature at the compressor outlet (T_{oc});

$y_5(t)$, temperature at the turbine outlet (T_{ot});

$y_6(t)$, electrical power at the generator terminal (P_e).

Simulated Application Examples (Cont'd)

Simulated Gas Turbine (SIMULINK®)

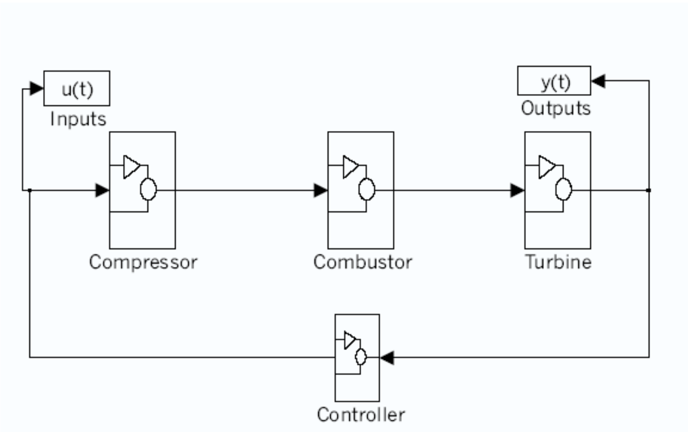

Figure 5.7: SIMULINK block diagram of the process.

Gas turbine main cycle parameters (ISO design conditions).

Air mass flow rate [kg/s]	24.4
Cycle pressure ratio (P_{oc}/P_{ic})	9.1
Electrical power (P_e) [kW]	5220
Exhaust temperature (T_{ot})[K]	796
Fuel mass flow rate (M_f) [kg/s]	0.388
IGV angle range ($\Delta\alpha$) [deg]	17

Simulated Application Examples (Cont'd)

Simulated Power Plant: *Pont sur Sambre*

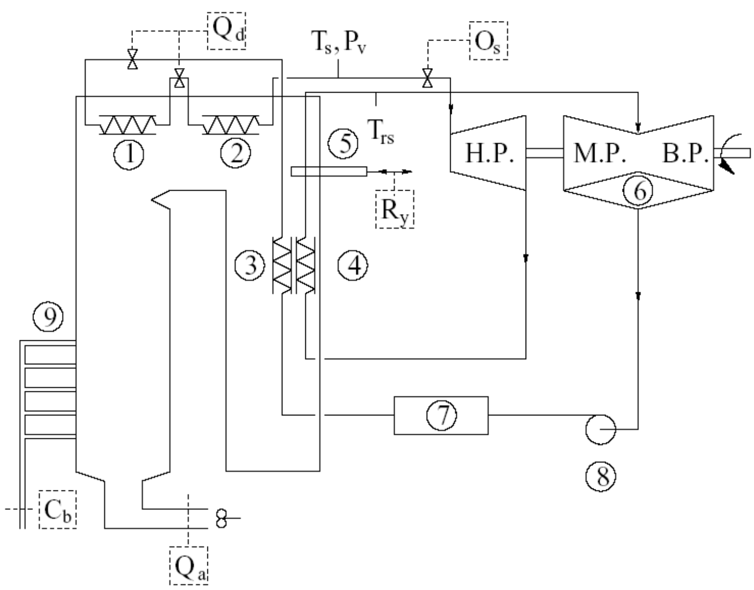

1. super heater (radiation);
2. super heater (convection);
3. super heater;
4. reheater;
5. dampers;
6. condenser;
7. drum;
8. water pump;
9. burner.

Simulated Application Examples (Cont'd)

Simulated Power Plant: *Pont sur Sambre*

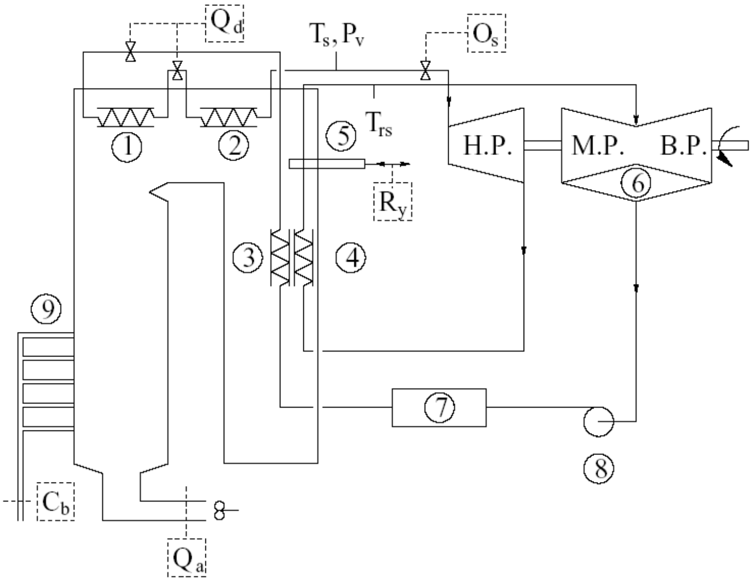

$u_1(t)$	C_b	gas flow
$u_2(t)$	O_s	turbine valves opening
$u_3(t)$	Q_d	super heater spray flow
$u_4(t)$	R_y	gas dampers
$u_4(t)$	Q_a	air flow
$y_1(t)$	P_v	steam pressure
$y_2(t)$	T_s	main steam temperature
$y_i(t)$	T_{rs}	reheat steam temperature

Simulated Application Examples (Cont'd)

Simulated Gas Turbine

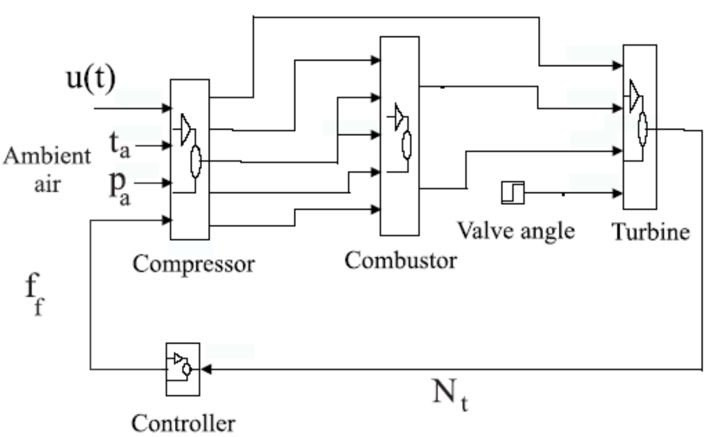

Figure 5.44: The monitored system.

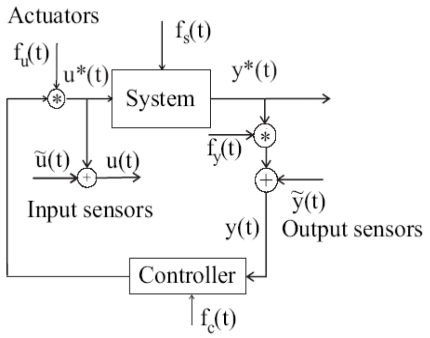

Figure 5.46: Turbine closed–loop scheme.

Simulated Application Examples (Cont'd)

Small Aircraft Model

Table 1: Nomenclature

V	True Air Speed (TAS)	H	altitude
α	angle of attack	δ_e	elevator deflection angle
β	angle of sideslip	δ_a	aileron deflection angle
P	roll rate	δ_r	rudder deflection angle
Q	pitch rate	δ_{th}	throttle aperture percentage
R	yaw rate	γ	flight path angle
ϕ	bank angle	g	acceleration of gravity
θ	elevation angle	m	airplane mass
ψ	heading angle	I_x, I_y, I_z	principal-axis inertia moments
n	engine shaft angular rate	d_t	distance of c.g. from the Thrust line

Piper Malibu

Simulated Application Examples (Cont'd)

Small Aircraft Model

Table 1: Nomenclature

V	True Air Speed (TAS)	H	altitude
α	angle of attack	δ_e	elevator deflection angle
β	angle of sideslip	δ_a	aileron deflection angle
P	roll rate	δ_r	rudder deflection angle
Q	pitch rate	δ_{th}	throttle aperture percentage
R	yaw rate	γ	flight path angle
ϕ	bank angle	g	acceleration of gravity
θ	elevation angle	m	airplane mass
ψ	heading angle	I_x, I_y, I_z	principal-axis inertia moments
n	engine shaft angular rate	d_t	distance of c.g. from the Thrust line

Simulated Application Examples (Cont'd)

6.1 SATELLITE OVERVIEW

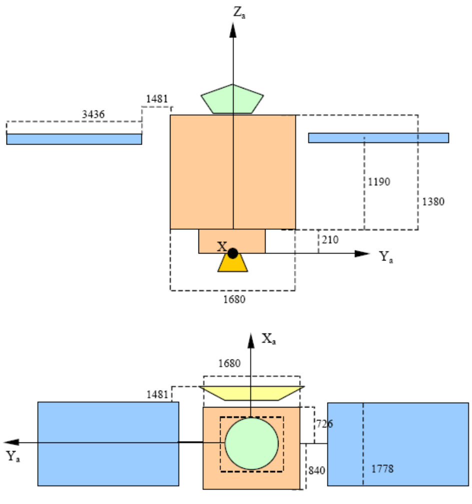

Figure 6-1: Satellite dimensions

6.4 SOLAR ARRAYS DYNAMICS

A GLOBALSTAR solar array has been selected. Its dimensions are recalled on the Figure 6-2.

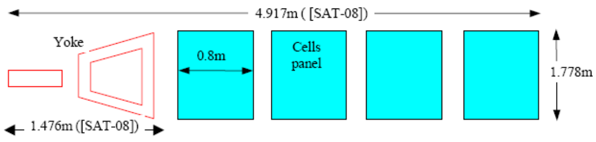

Figure 6-2 : MARS-EXPRESS solar array

Simple SA model

Aerospace Satellite

Simulated Application Examples (Cont'd)

Aerospace Satellite

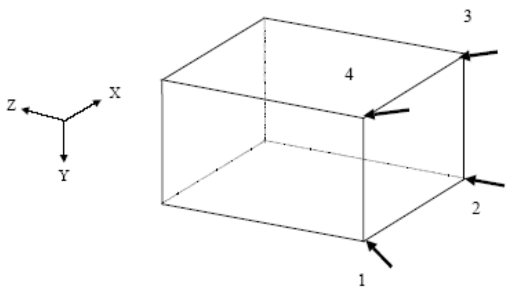

Figure 6-3 : Thrusters implementation

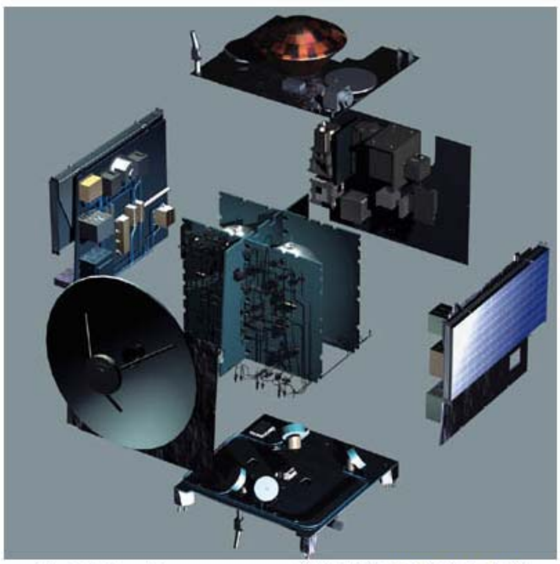

Fig. 1: Mars Express spacecraft (MEX) (www.esa.int)

Fault Diagnosis Application Studies

Gas Turbine FDI (*1*)

- MIMO SIMULINK model of a real single-shaft industrial gas turbine with variable Inlet Guided Vane (IGV) angle working in parallel with electrical mains

Block diagram of the gas turbine model

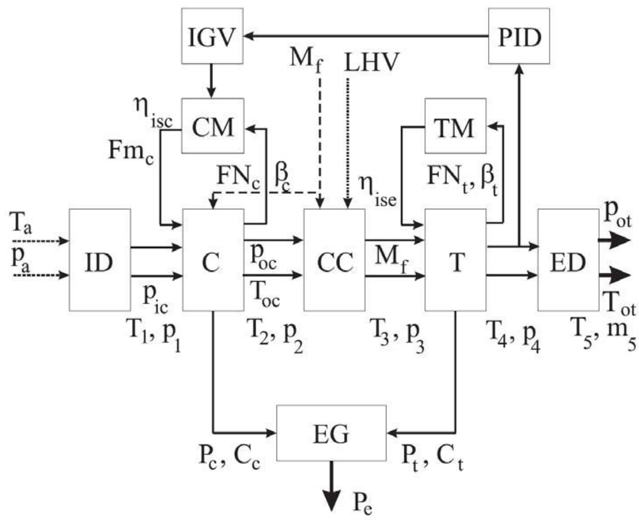

SIMULINK Model Validation

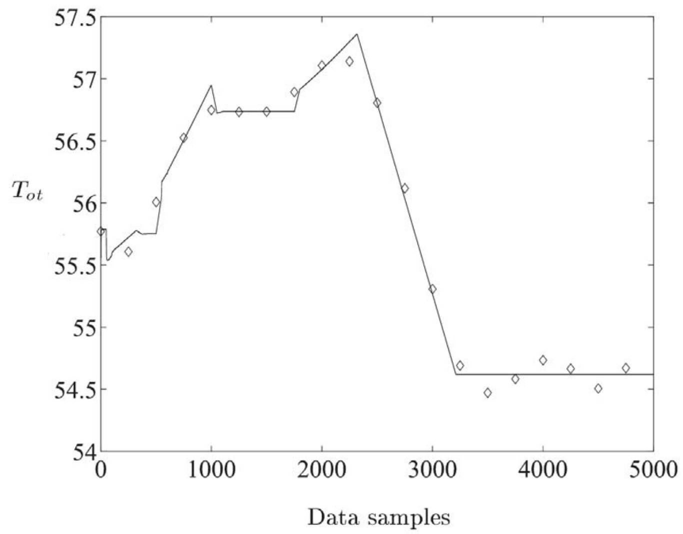

Fig. 5.3. Turbine outlet temperature T_{ot} in the case of load reduction performed reducing the fuel flow rate M_f and closing the IGV angle α.

SIMULINK Model Validation (Cont'd)

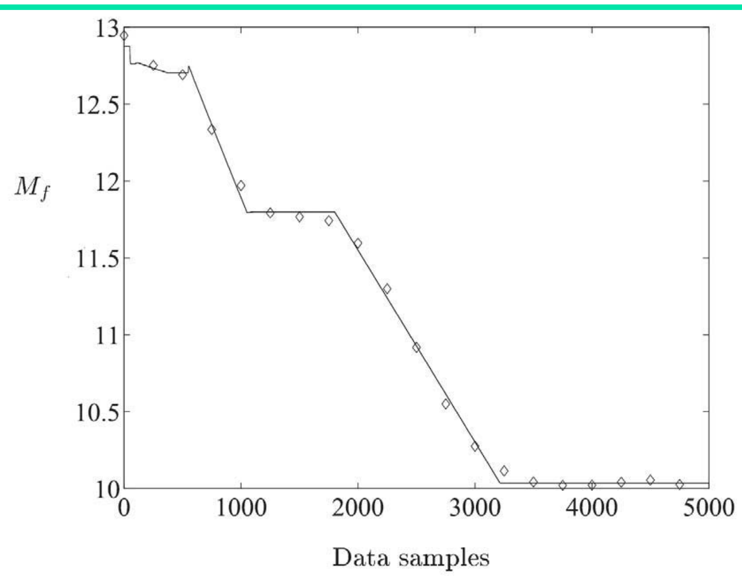

Fig. 5.4. Fuel flow rate M_f in the case of load reduction performed reducing the fuel flow rate M_f and closing the IGV angle α.

SIMULINK Model Validation (Cont'd)

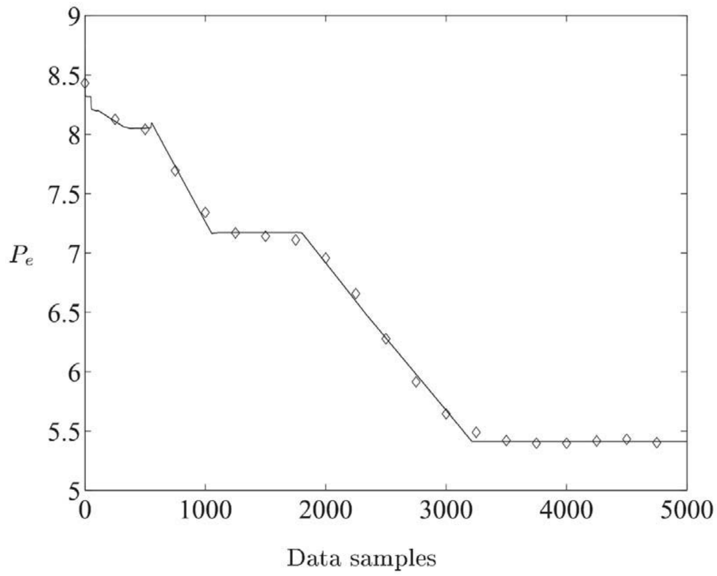

Fig. 5.5. Electrical power P_e in the case of load reduction performed reducing the fuel flow rate M_f and closing the IGV angle α.

SIMULINK Model Identification

- Inputs

$u_1(t)$, Inlet Guide Vane (IGV) angular position (α);
$u_2(t)$, fuel mass flow rate (M_f).

- Outputs

$y_1(t)$, pressure at the compressor inlet (p_{ic});
$y_2(t)$, pressure at the compressor outlet (p_{oc});
$y_3(t)$, pressure at the turbine outlet (p_{ot});
$y_4(t)$, temperature at the compressor outlet (T_{oc});
$y_5(t)$, temperature at the turbine outlet (T_{ot});
$y_6(t)$, electrical power at the generator terminal (P_e).

SIMULINK Model Signals

Table 5.1. Gas turbine main cycle parameters (ISO design conditions).

Air mass flow rate [kg/s]	24.4
Cycle pressure ratio (P_{oc}/P_{ic})	9.1
Electrical power (P_e) [kW]	5220
Exhaust temperature (T_{ot})[K]	796
Fuel mass flow rate (M_f) [kg/s]	0.388
IGV angle range ($\Delta\alpha$) [deg]	17

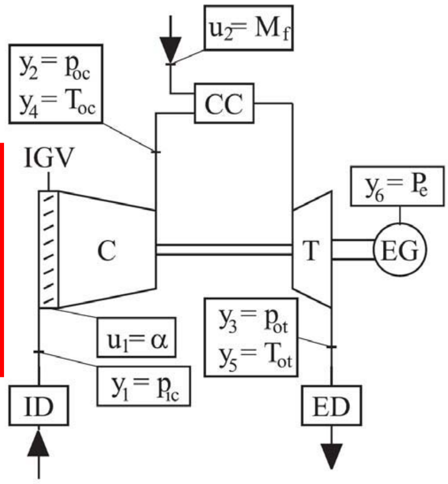

Fig. 5.6. Layout of the single–shaft industrial gas turbine with the monitored sensors highlighted.

Gas Turbine Simulator

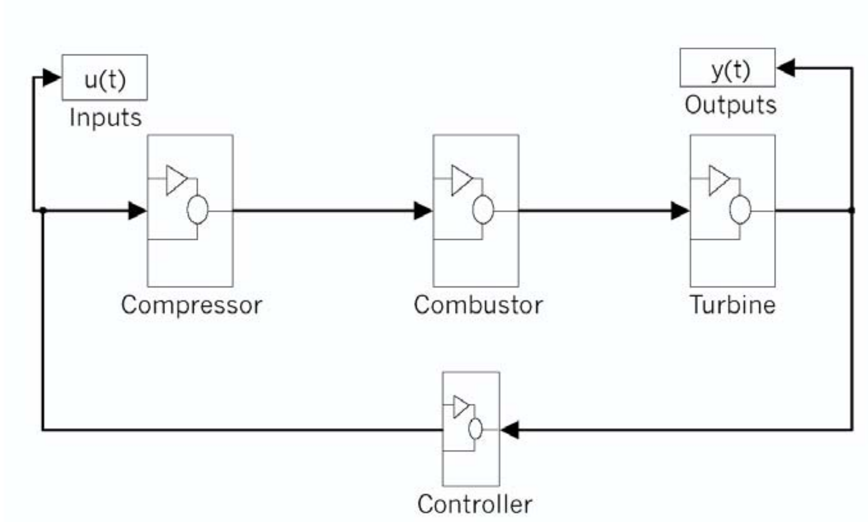

Fig. 5.7. SIMULINK block diagram of the process.

Gas Turbine Inputs (with noise)

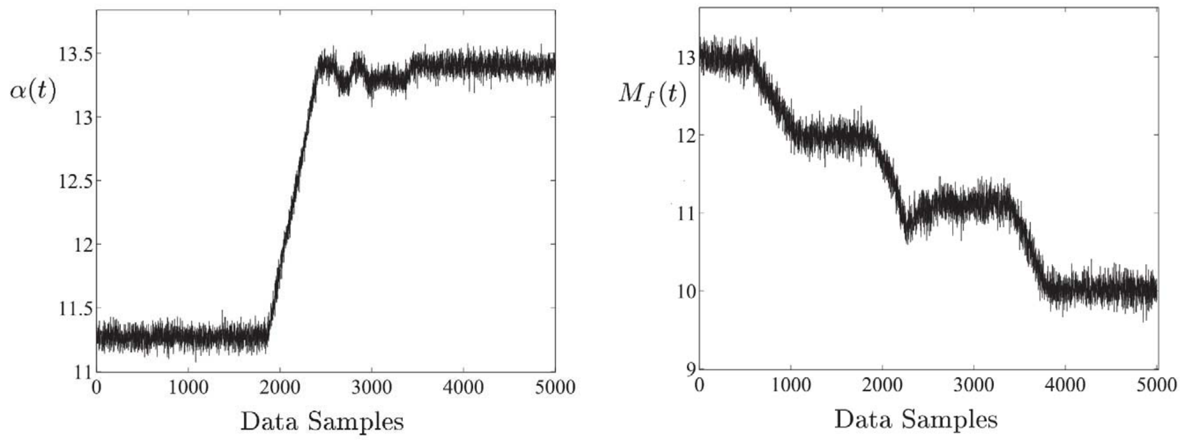

(a) First input, $\alpha(t)$ (b) Second input, $M_f(t)$

Gas Turbine Outputs (with noise, Cont'd)

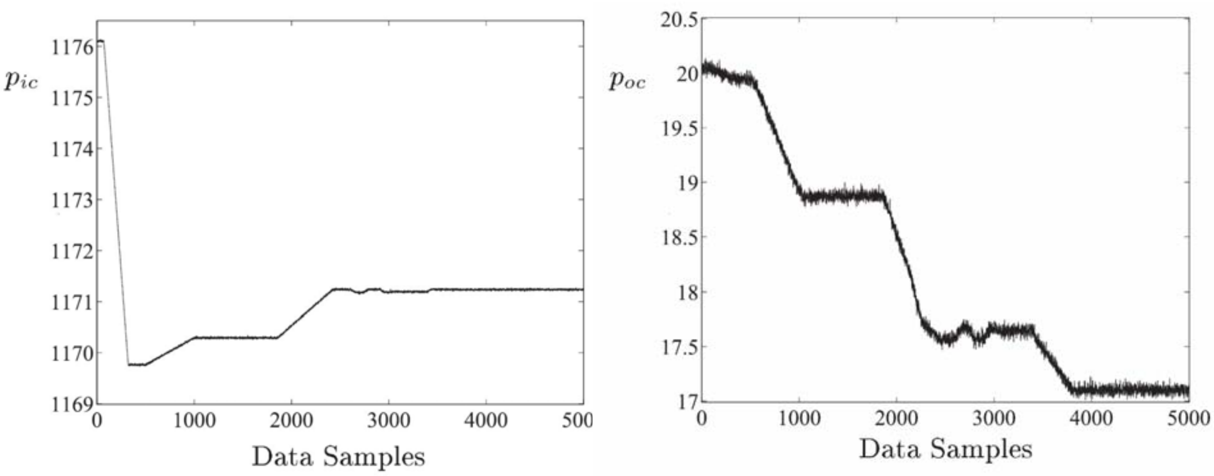

(a) First output, p_{ic} (b) Second output, p_{oc}

Gas Turbine Outputs (with noise, Cont'd)

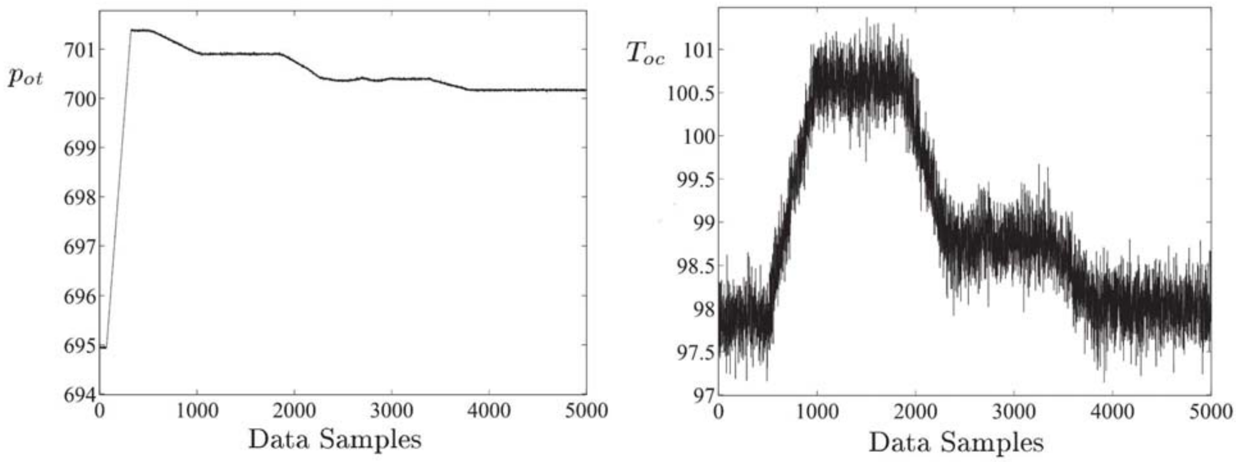

(a) Third output, p_{ot} (b) Fourth output, T_{oc}

Gas Turbine Outputs (with noise, Cont'd)

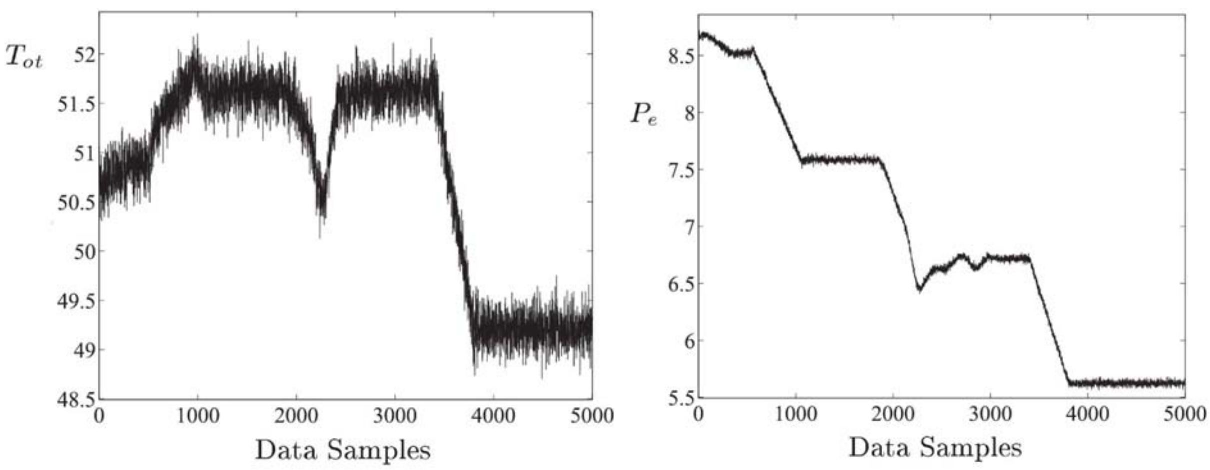

(a) Fifth output, T_{ot} (b) Sixth output, P_e

Parameter Variations

- Table 5.2 shows the parameter variations of the input-output model relative to the p_{ic} measurement versus the measurement noise

Table 5.2. Parameter variation of the p_{ic} ARX model versus measurement noise.

Noise	0 %	2 %	10 %	20 %
α_2	−0.9963	−0.9941	−0.9513	−0.9325
α_1	1.9963	1.9949	1.9712	1.9486
β_{11}	0.9205	0.9368	0.9680	0.9458
β_{12}	−0.9176	−0.9455	−0.9682	−0.9864
β_{21}	0.0044	0.0178	0.0176	0.0220
β_{22}	−0.0044	−0.0092	−0.0108	−0.0197

OO Design Example

MATLAB

```
» A =[1.8097 -0.8187; 1 0];
» B = [0.5; 0];
» C =[0.1810 -0.1810];
» D = 0;

» L=place(A',C',[.5 .7])'

» eig(A-L*C)
ans = 0.7000 0.5000
```

State-space model in discrete-time

$$A = \begin{bmatrix} 1.8097 & -0.8187 \\ 1 & 0 \end{bmatrix}, \; B = \begin{bmatrix} 0.5 \\ 0 \end{bmatrix}$$
$$C = \begin{bmatrix} 0.1810 & -0.1810 \end{bmatrix}, \; D = 0$$

Resulting observer gain

$$L = \begin{bmatrix} -82.6341 \\ -86.0031 \end{bmatrix}$$

Double-check observer poles: answer is ok !

UIO Design Example

```
A = [0.9944 -0.1203  -0.4302;
     0.0017  0.9902  -0.0747;
     0       0.8187   0];

B = [0.4252 -0.0082 0.1813]';

E = [1 0;
     0 1;
     0 0];

C = eye(3);
D = zeros(3,3);

v = [0.75 0.80 0.85];
```

```
H = E*pinv(C*E);

T = eye(size(H*C)) - H*C;

K1 = place( (A-H*C*A)' , C', v )';

F = A-H*C*A - K1*C;

K2  = F*H;

K = K1 + K2;
```

$$\begin{cases} z(t+1) = F\,z(t) + T\,B\,u(t) + K\,y(t) \\ \hat{x}(t) = z(t) + H\,y(t) \end{cases}$$

Gas Turbine FDI

- Fault detection thresholds
- Fault-free residuals ± 10% margins

Table 5.3. Fault detectability thresholds.

Measurement	Positive threshold	Negative threshold
T_{oc}	+0.85	-0.85
T_{ot}	+0.20	-0.22
p_{ot}	+0.022	-0.024
p_{oc}	+0.55	-0.65
p_{ic}	+0.022	-0.0225
P_e	+2.0	-2.2
M_f	+1.1	-1.1
α	+0.27	-0.41

Gas Turbine FDI (UIO)

- Fault-free residual generated by the UIO driven by the signal of M_f input sensor and that it is insensitive to the signal of the IGV input sensor
- The eigenvalues of the state distribution matrix of the UIO are placed near to 0.2

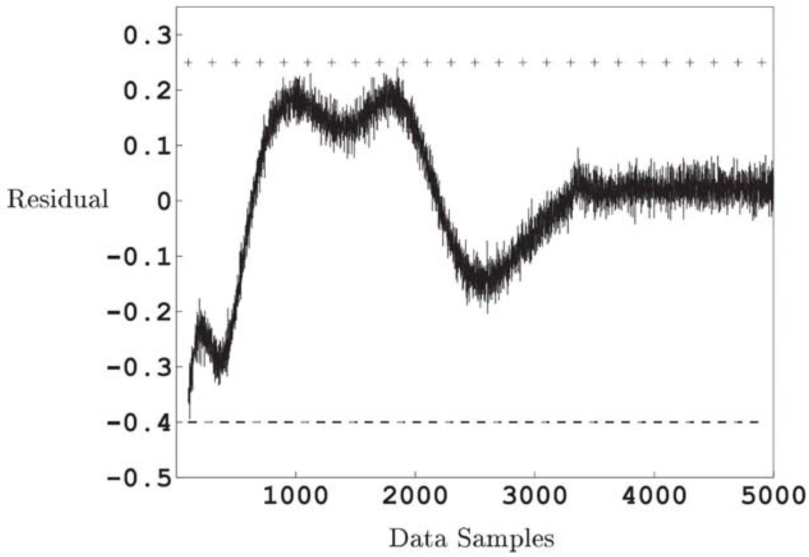

Gas Turbine FDI (UIO, Cont'd)

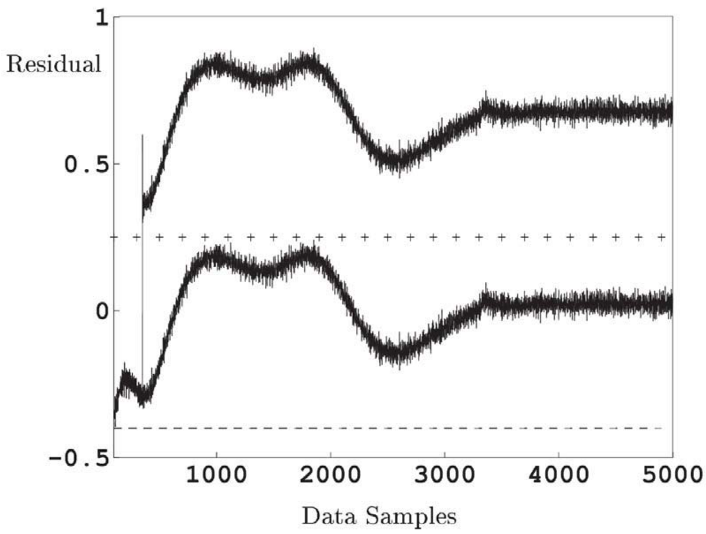

Fig. 5.13. Residual function of the UIO driven by the M_f signal in the presence of an additive positive fault signal.

Gas Turbine FDI (UIO, Cont'd)

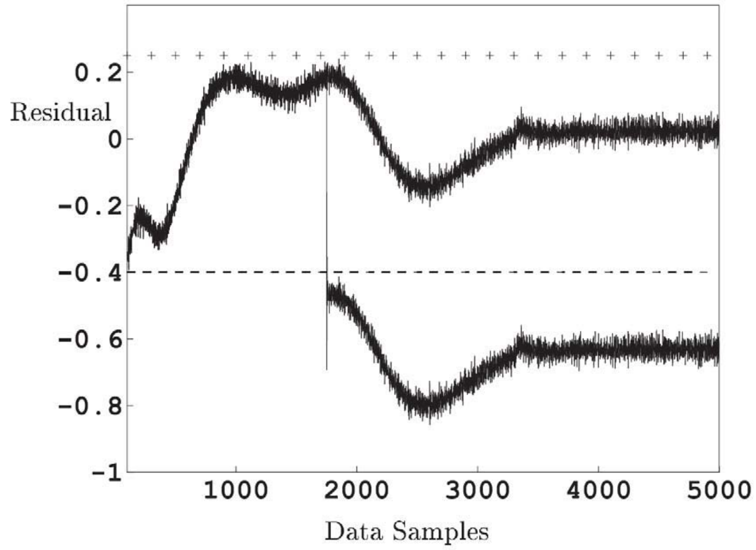

Fig. 5.14. Residual function of the UIO driven by the M_f signal in the presence of an added negative fault signal.

Gas Turbine FDI (OO, Cont'd)

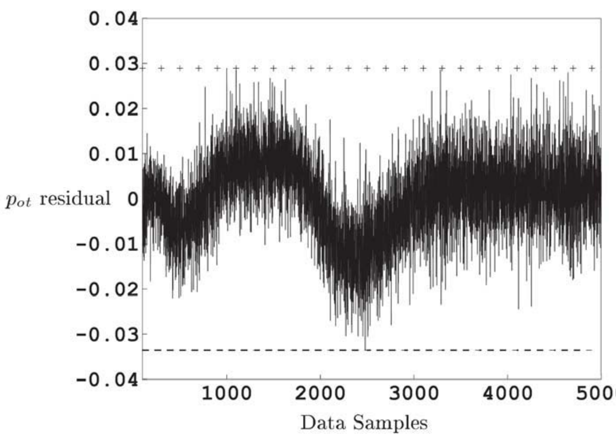

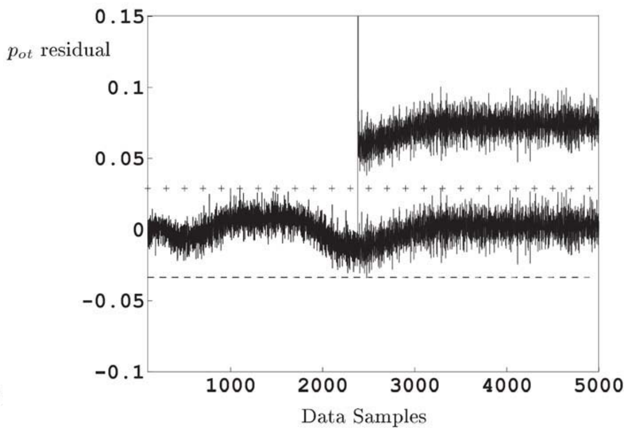

Fig. 5.16. Residual function of output observer driven by p_{ot} signal with an added positive fault signal.

Gas Turbine FDI (OO, Cont'd)

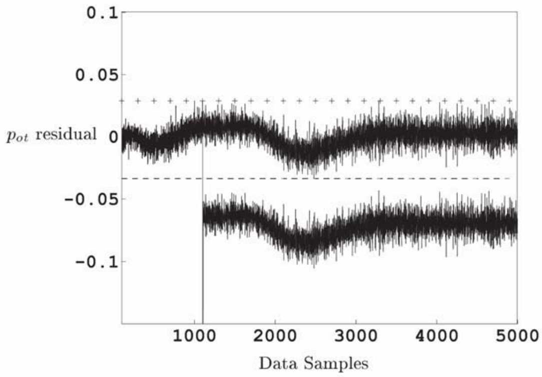

Fig. 5.17. Residual function of output observer driven by p_{ot} signal with negative failure.

Minimal detectable step faults

Table 5.4. Minimal detectable step faults.

α	M_f	p_{ic}	p_{oc}	p_{ot}	T_{oc}	T_{ot}	P_e
4%	4%	5%	7%	5%	5%	2.5%	1.7%

Gas Turbine FDI (Ramp Faults)

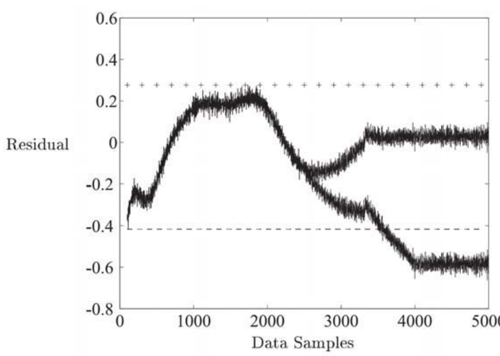

Fig. 5.18. Residual function of the UIO driven by the α signal in the presence of a drift in the α measurement.

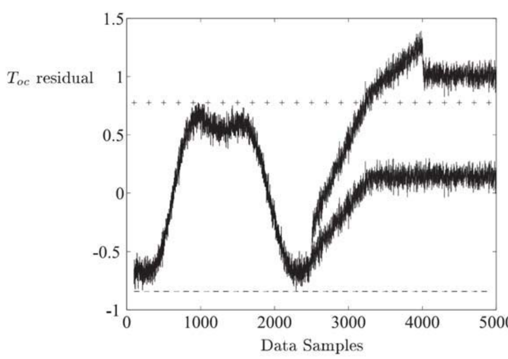

Fig. 5.19. Output observer residual signal T_{oc} corresponding to a drift in the T_{oc} measurement.

FDI with UIO and OO: Examples

Minimum Detectable Ramp Faults

Table 5.5. Minimal detectable ramp faults.

Measurement	Fault	Detection delay [s]
T_{oc}	5 %	50
T_{ot}	3 %	100
p_{ot}	5.5 %	75
p_{oc}	7.5 %	0
p_{ic}	6 %	50
P_e	6 %	100
M_f	4 %	150
α	4 %	100

FDI with Kalman Filters

- Kalman Filters for residual generation
  - Set of measured variables of the system compared with the corresponding signals estimated by the KFs to generate residual functions
- The diagnosis can be performed by detecting the changes of these residuals caused by a fault
  - The fault diagnosis of input sensors uses a number of KF equal to the number of input variables
  - Each KF is designed to be insensitive to a different input of the system
  - Output sensor faults are detected by means of a classic KF, driven by a single output and all the inputs of the system

KF Design Example

```
A = [1.1269   -0.4940    0.1129
     1.0000         0         0
          0    1.0000         0];

B = [-0.3832
      0.5919
      0.5191];

C = [1 0 0];

D = zeros(1,2);
```


KF Design Example (Cont'd)

```
Plant = ss(A,[B B],C,0,-1,'inputname',{'u'
   'w'},'outputname','y');

%%% Note: set sample time to -1 to mark model
%%% as discrete

Q = 1; R = 1; %%% Assuming that Q = R = 1;

[kalmf,L,P] = kalman(Plant,Q,R);
```

KF for FDI

- Because of the linear property of the identified model and because of the additive effect of the faults on the system, it may easily be shown that the effect of the change on the innovation is also additive
- Any abrupt change in measurements due to a fault is reflected in a change in the mean value and in the standard deviation of innovations

KF for FDI (Cont’d)

- KF produces zero-mean and independent white residuals with the system in normal operation
- Testing how much the sequence of innovations has deviated from the white noise hypothesis
- Tests which performed on the innovations $r(t)$ are the usual ones for zero-mean and variance, in the form of cumulative sum algorithms

KF for FDI (Cont'd)

Residual mean value and variance

$$\overline{r}(t) = E[r(t)] = \frac{1}{t}\sum_{j=1}^{t} r(j)$$

$$\sigma_r^2(t) = E[r^2(t)] = \frac{1}{t}\sum_{j=1}^{t} r^2(j)$$

KF for FDI (Cont'd)

Residual whiteness: χ^2 test

$$\begin{aligned} R_r^t(\tau) &= \frac{1}{t}\sum_{j=1}^{t} r(j)r(j+\tau), \\ \zeta_r^M(t) &= \frac{t}{R_r^t(0)^2}\sum_{\tau=1}^{M}\left(R_r^t(\tau)\right)^2 \end{aligned}$$

FDI with Kalman Filters

- If a system abnormality occurs, the statistics of *r(t)* change, so the comparison of *r(t)* and with a threshold ε fixed under no faults conditions, becomes the detection rule
- Such a threshold can be settled the aid of χ^2 tables that can be computed as a function of the false-alarms probability β and of the window size M

FDI with Kalman Filters (Cont'd)

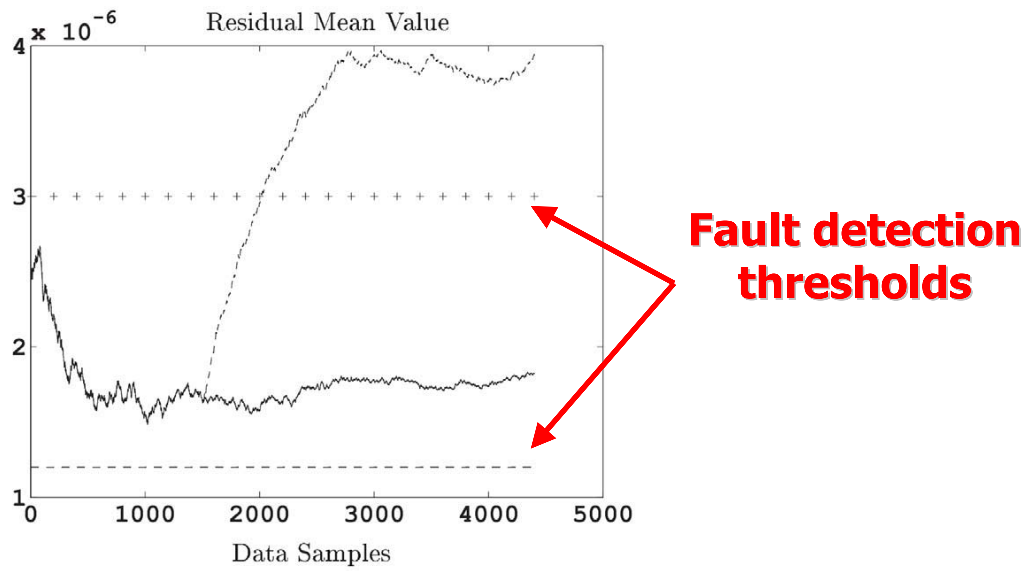

Fig. 5.20. Mean value of the residual computed by using KF with unknown input in a growing window.

FDI with Kalman Filters (Cont'd)

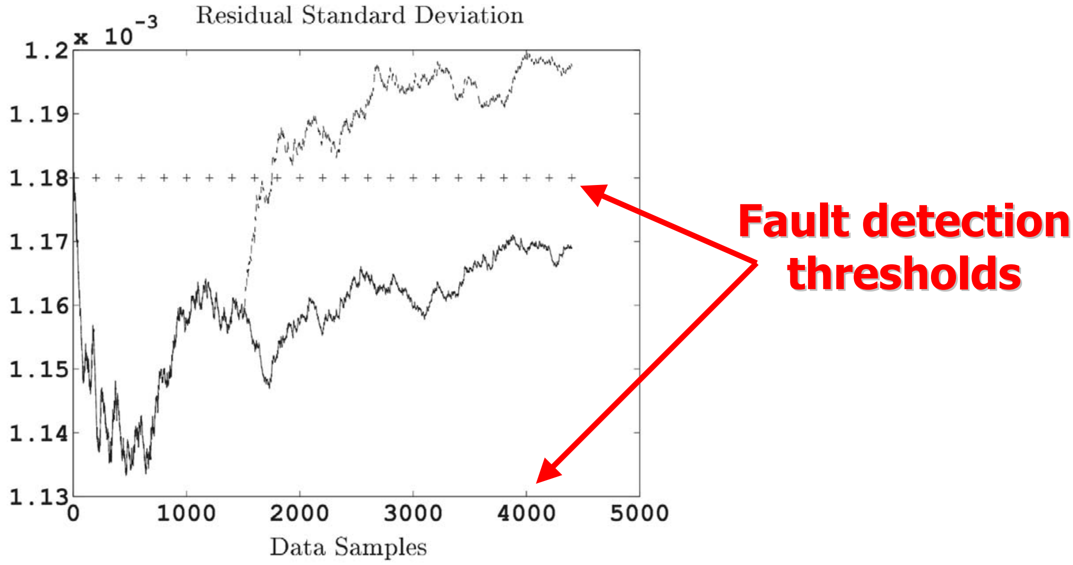

Fig. 5.21. Standard deviation of the residual computed by using a KF with unknown input in a growing window.

FDI with Kalman Filters (Cont'd)

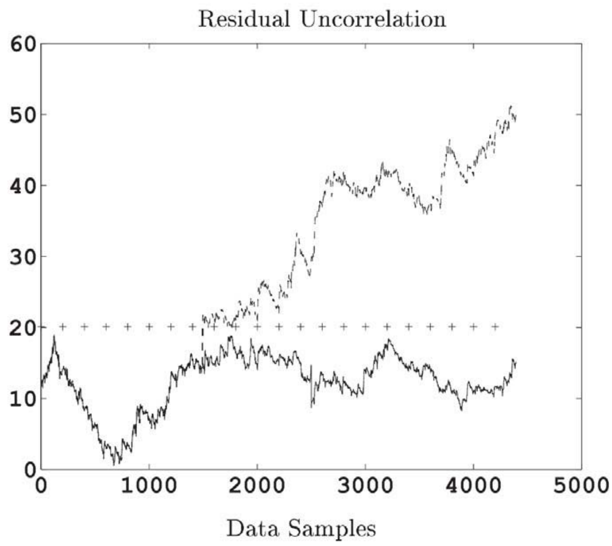

Fig. 5.22. Residual uncorrelation computed using a KF with unknown input in a growing window.

FDI with Kalman Filters (Cont'd)

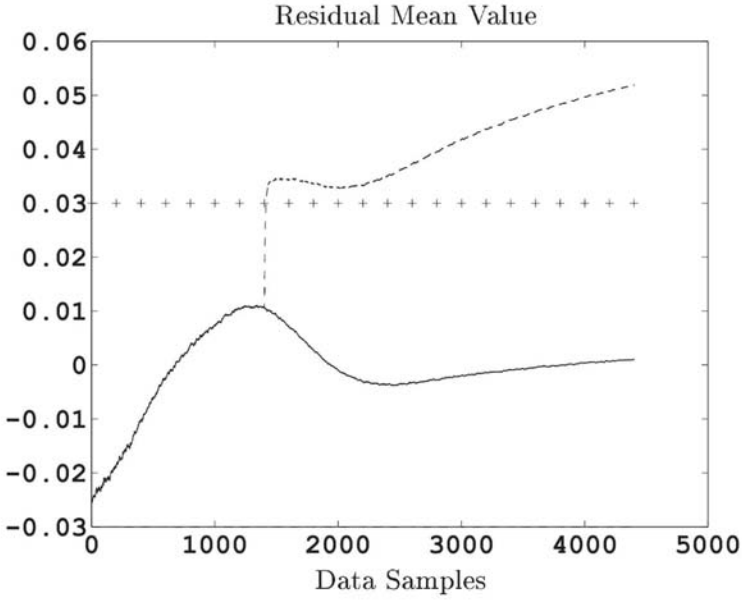

Fig. 5.23. Mean value of the p_{ic} residual computed by using a growing window.

FDI with Kalman Filters (Cont'd)

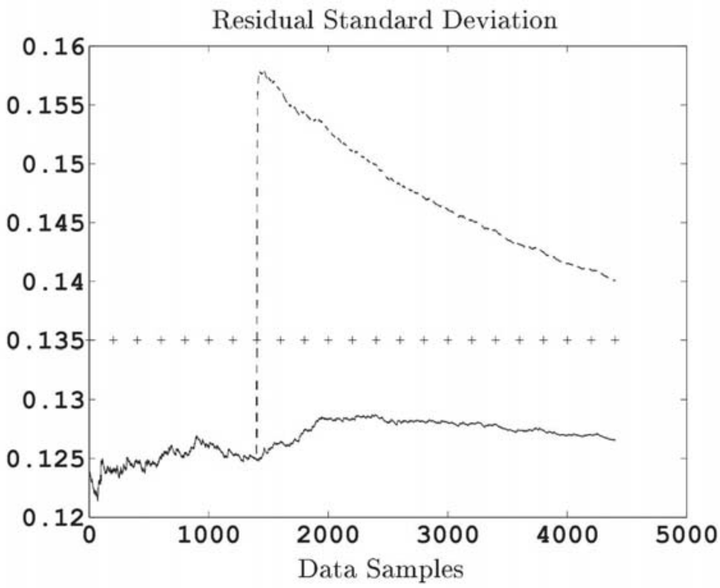

Fig. 5.24. Standard deviation of the p_{ic} residual computed by using a growing window.

FDI with Kalman Filters (Cont'd)

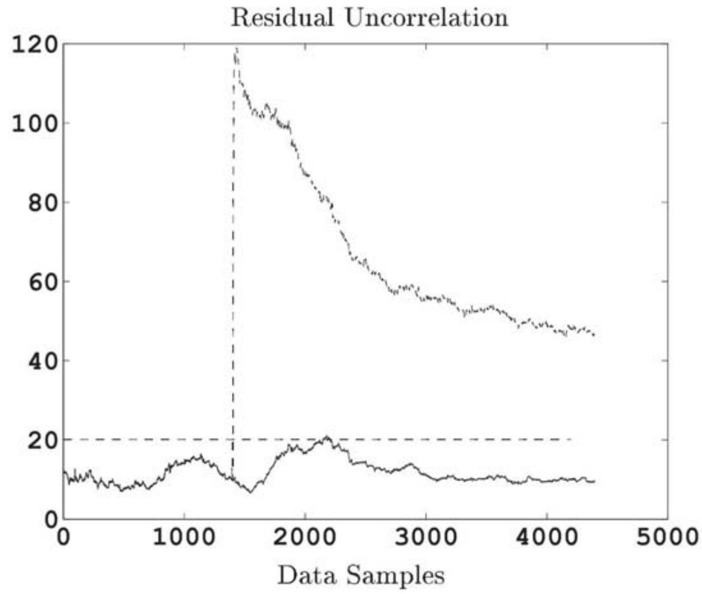

Fig. 5.25. Uncorrelation of the p_{ic} residual computed by using a growing window.

Minimal Detectable Faults

Table 5.7. Minimum detectable faults by monitoring residual mean value.

α	M_f	p_{ic}	p_{oc}	p_{ot}	T_{oc}	T_{ot}	P_e
3%	3%	2.5%	4%	1.5%	2%	2.5%	3%

Table 5.8. Minimum detectable faults by monitoring residual uncorrelation.

α	M_f	p_{ic}	p_{oc}	p_{ot}	T_{oc}	T_{ot}	P_e
2%	2.5%	0.75%	1%	0.75%	2%	0.8%	1.5%

FDI with Fuzzy Systems

$$R_i: \quad \textbf{IF } \boldsymbol{x}(t) \text{ is } A_i \text{ THEN } y_i = f_i(\boldsymbol{x}(t)), \quad i = 1, 2, \cdots, K,$$

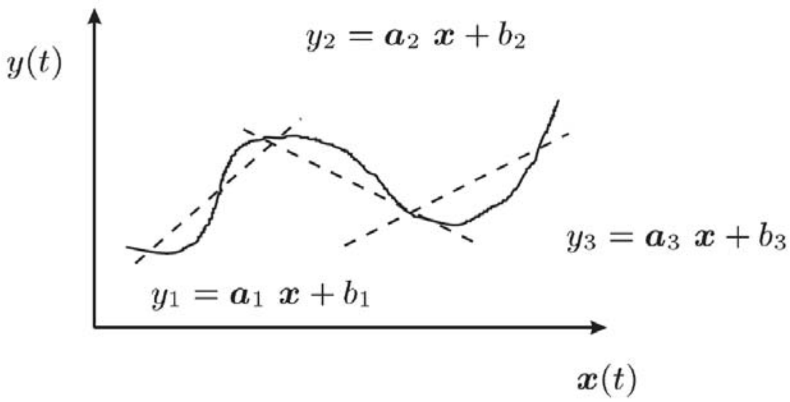

Residuals from Fuzzy Models

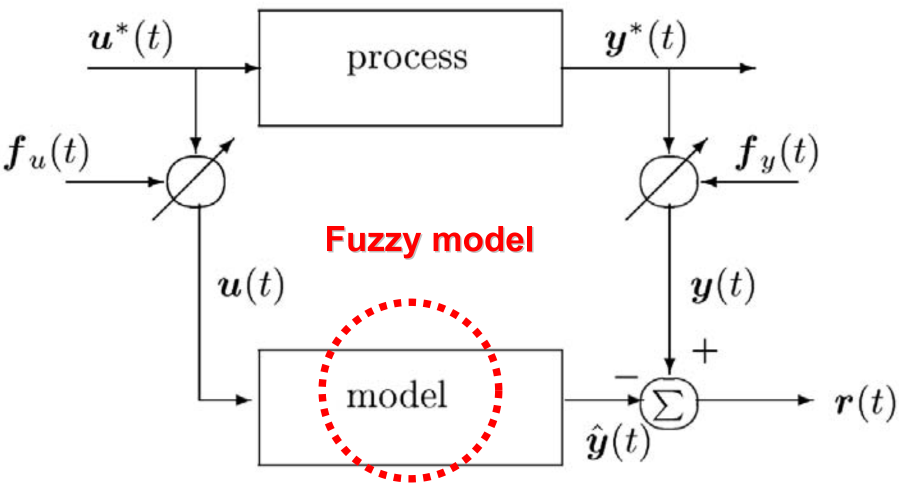

Fig. 4.8. The residual generation scheme.

Fuzzy Identification Details

- The GK clustering algorithm was used with $M = 3$ clusters (operating conditions) and $n = 2$ the number of sample delays of the inputs and outputs
- After clustering, the system parameters θ_i with $i = 1, \ldots, M$ for each output, were estimated using LSM

Fuzzy FDI Results

- Mean square estimation errors

Table 5.9. Output estimation errors with and without the multiple–model approach.

Output	p_{ic}	p_{oc}	p_{ot}	T_{oc}	T_{ot}	P_e
Classical observer	13.29	7.56	15.34	20.22	21.57	19.70
Fuzzy model	2.04	3.22	1.67	2.55	2.58	1.70

- Comparisons (minimal detectable faults)

Table 5.10. Minimal detectable step faults with and without the multiple–model approach.

Sensor	α	M_f	p_{ic}	p_{oc}
Classical observer	4%	4%	5%	7%
Fuzzy model	1.8%	2.3%	0.60%	0.8%
Sensor	p_{ot}	T_{oc}	T_{ot}	P_e
Classical observer	5%	5%	2.5%	1.7%
Fuzzy model	0.65%	1.7%	0.65%	1.2%

Fuzzy FDI Results (Cont'd)

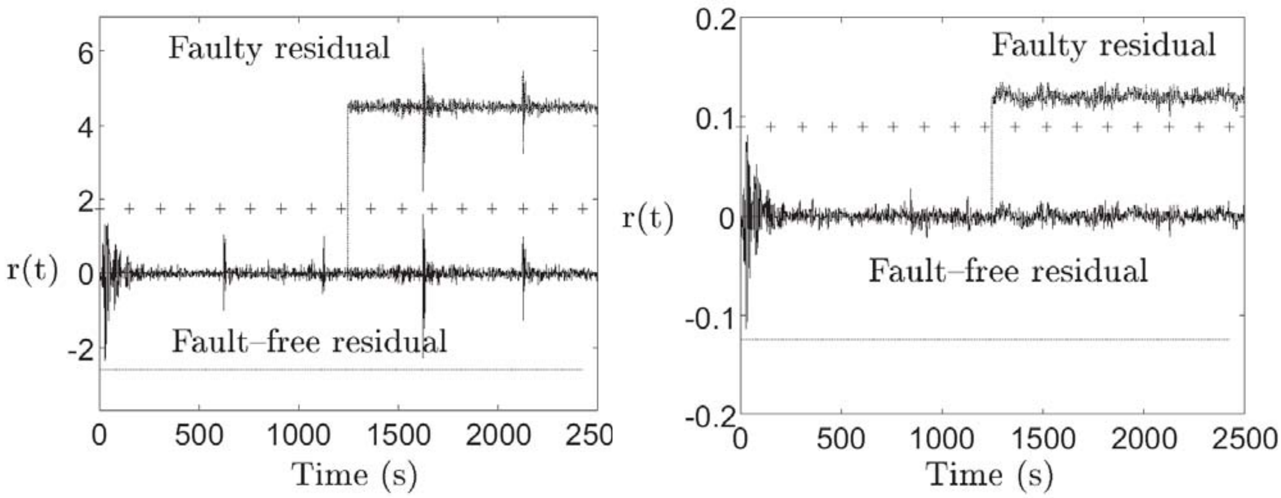

Observer vs. fuzzy model

FDI with Neural Networks

- Identification of faults regarding control sensors of the single shaft industrial gas turbine
- Faults modelled by step functions create changes in several residuals obtained by using dynamic observers
- NN is exploited to find the connection from a particular fault regarding input and output sensors to a particular residual

Fault Identification via NN

- Observers generate residuals that do not depend on the dynamic characteristics of the plant, but only on sensors faults
- NN classifies static patterns of residuals, which are uniquely related to particular fault conditions independently from the plant dynamics
- A number of residuals equal to the number of the outputs of the process is obtained by the difference between the estimated measurements computed by observers and the real measurements

Fault Identification via NN (Cont'd)

- The identification of output sensor faults is indeed very easy, since each output measurement is directly connected to a single residual generator
- This situation does not hold for the inputs, and the relation between input faults and residuals should be determined
- The solution to this problem was obtained by exploiting the learning capabilities of a NN
- Find the relationships that exist between input sensor faults and residuals

Fault Identification via NN (Cont'd)

- The classification method is typically an off-line procedure in which the fault mode is first defined and the data (residuals) are then collected
- The classification of process residuals can be carried out in accordance with the information about different faults
- It is known that certain residual patterns correspond to the normal operation and other patterns correspond to the faulty operation

Fault Identification via NN (Cont'd)

- With this kind of data the training of the NN is performed
- The NN implemented by the Neural Network Toolbox for MATLAB are Multi-layer Perceptron and Radial Basis Function NN
- Able to approximate any continuous function with an arbitrary degree of accuracy, provided with a sufficient number of neurons

Network Training

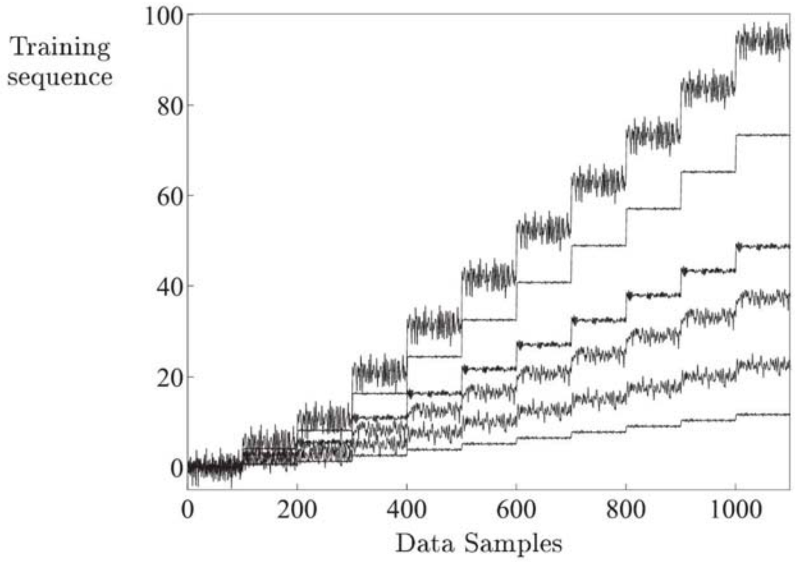

- One residual for each output (6)
- 11 fault sizes simulated
- 6 inputs for the NN

Fig. 5.27. NN input pattern.

Network Training (Cont'd)

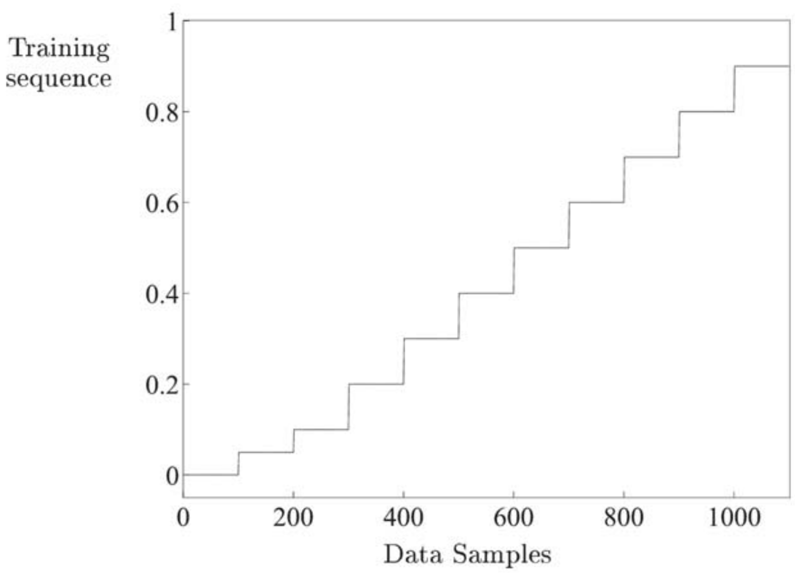

- One signal
- 11 fault sizes
- 1 output for the NN (target)

Fig. 5.28. Output pattern of the NN.

NN Training Results

- SSE = sum of square errors (of the neural network)

Table 5.11. Training results concerning the M_f sensor.

Input layer	Hidden layer	SSE after 70000 epochs
15	15	0.27
15	20	0.264
20	50	**0.127**

Table 5.12. Training results concerning the IGV sensor.

Input layer	Hidden layer	SSE after 70000 epochs
15	15	0.17
15	20	0.24
20	30	**0.108**

Table 5.13. Minimal detectable step faults.

Method	M_f	IGV
(NN)	3%	2.5%

Power Plant FDI (*2*)

- MIMO real 120MW power plant of Pont sur Sambre. It is a double-shaft industrial gas turbine working in parallel with electrical mains

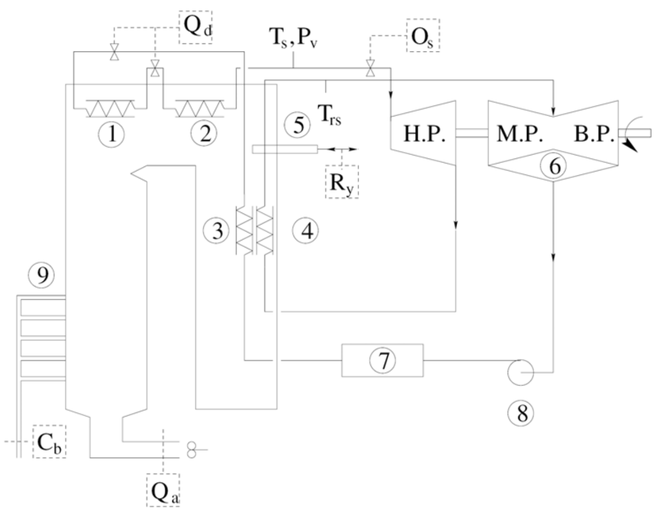

1. super heater (radiation);
2. super heater (convection);
3. super heater;
4. reheater;
5. dampers;
6. condenser;
7. drum;
8. water pump;
9. burner.

MIMO Power Plant of Pont sur Sambre

***N* = *2200* samples:**

Inputs

$u_1(t)$	C_b	gas flow
$u_2(t)$	O_s	turbine valves opening
$u_3(t)$	Q_d	super heater spray flow
$u_4(t)$	R_y	gas dampers
$u_4(t)$	Q_a	air flow

T_s = 10 s.

Outputs

$y_1(t)$	P_v	steam pressure
$y_2(t)$	T_s	main steam temperature
$y_i(t)$	T_{rs}	reheat steam temperature

Plant Inputs (u_1 & u_2)

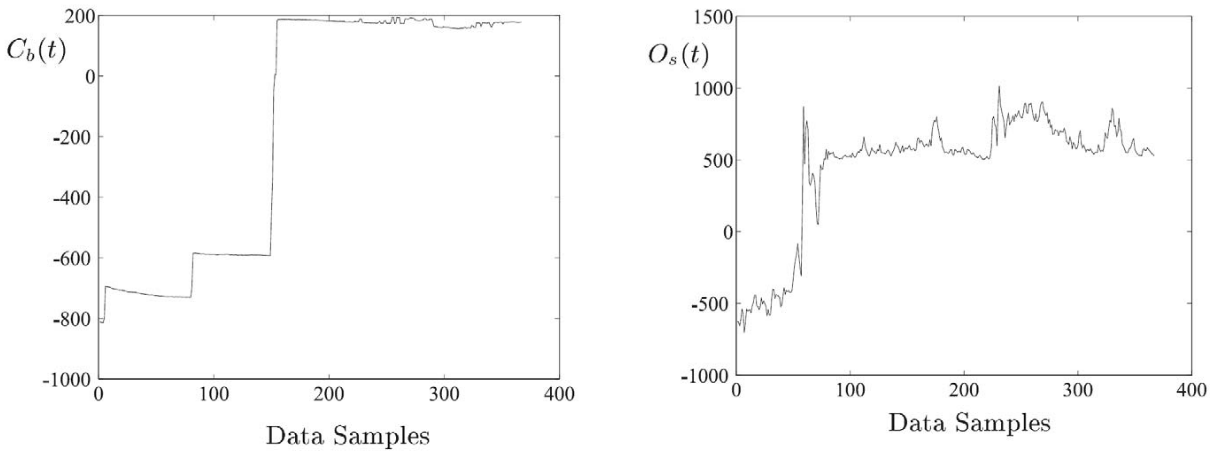

(a) First input, C_b

(b) Second input, O_s

Plant Inputs (u_3 & u_4)

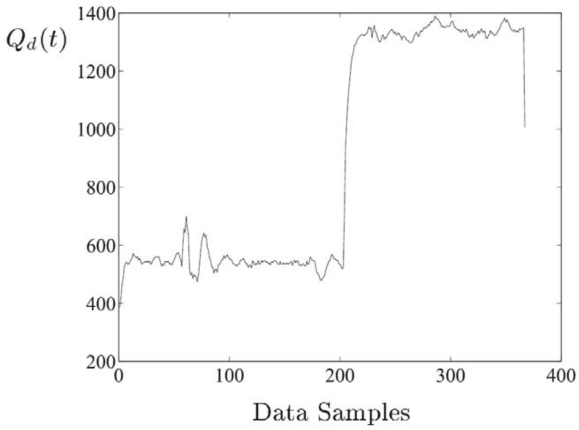

(a) Third input, Q_d

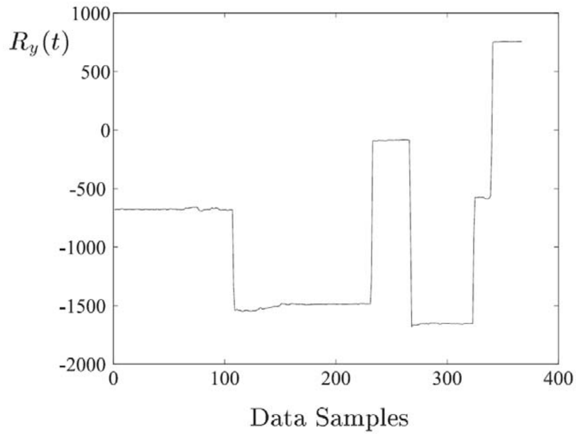

(b) Fourth input, R_y

Plant Input (u_5) and Output (y_1)

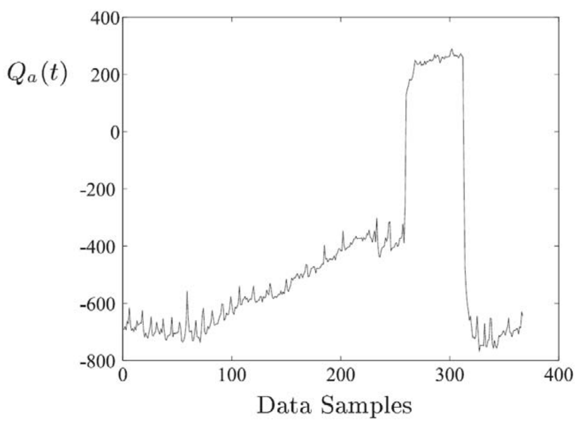

(a) Fifth input, Q_a

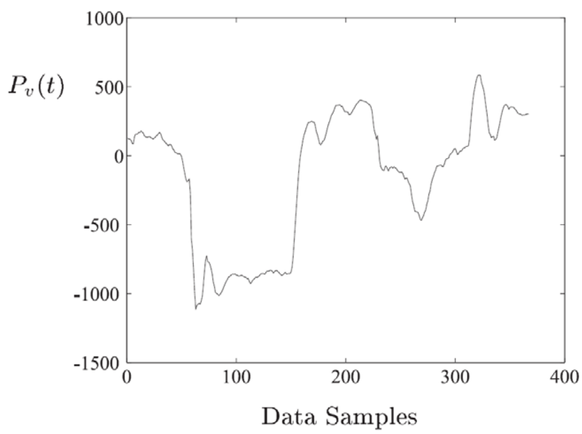

(b) First output, P_v

Plant Outputs (y_2 & y_3)

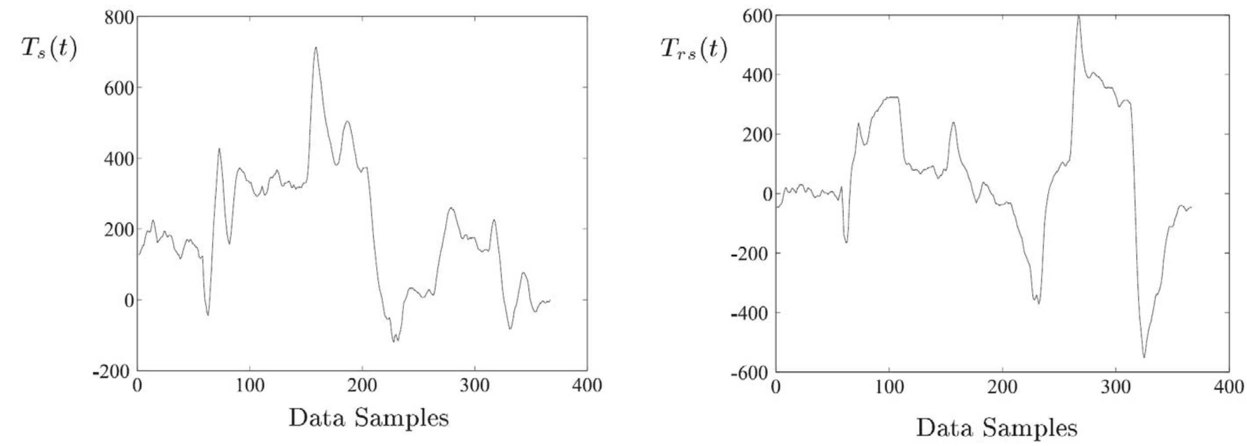

(a) Second output, T_s

(b) Third output, T_{rs}

Model Matrices: A & B

$$A = \begin{bmatrix} 0 & 0 & -2.19\,E-1 & 0 & 0 & -3.35\,E-1 & 0 & 0 & -1.85\,E-1 \\ 1 & 0 & 2.02\,E-1 & 0 & 0 & 4.75\,E-1 & 0 & 0 & 3.46\,E-1 \\ 0 & 1 & 9.45\,E-1 & 0 & 0 & -1.30\,E-1 & 0 & 0 & -1.27\,E-1 \\ 0 & 0 & 6.31\,E-2 & 0 & 0 & 8.30\,E-2 & 0 & 0 & -1.41\,E-1 \\ 0 & 0 & 1.94\,E-1 & 1 & 0 & -7.26\,E-1 & 0 & 0 & 2.87\,E-1 \\ 0 & 0 & -3.14\,E-1 & 0 & 1 & 1.63\,E\;0 & 0 & 0 & -1.16\,E-1 \\ 0 & 0 & -2.78\,E-2 & 0 & 0 & -3.00\,E-1 & 0 & 0 & 1.78\,E-1 \\ 0 & 0 & 4.18\,E-1 & 0 & 0 & 6.06\,E-1 & 1 & 0 & -9.03\,E-1 \\ 0 & 0 & -4.41\,E-1 & 0 & 0 & -2.13\,E-1 & 0 & 1 & 1.68\,E\;0 \end{bmatrix}$$

$$B = \begin{bmatrix} -1.70\,E-1 & 1.43\,E-1 & -4.32\,E-3 & -2.66\,E-3 & 3.32\,E-3 \\ -1.97\,E-1 & 1.62\,E-1 & -5.23\,E-2 & -1.55\,E-2 & 1.99\,E-1 \\ 2.77\,E-1 & 9.64\,E-3 & 3.72\,E-2 & 9.97\,E-3 & -1.10\,E-1 \\ -8.22\,E-2 & 7.30\,E-2 & 9.30\,E-2 & -1.34\,E-2 & -2.04\,E-2 \\ -1.66\,E-1 & 5.68\,E-2 & -4.20\,E-2 & -8.02\,E-6 & 6.50\,E-2 \\ 3.11\,E-1 & -1.24\,E-1 & 1.78\,E-2 & 3.78\,E-3 & -4.33\,E-2 \\ -3.85\,E-2 & -9.60\,E-3 & 4.77\,E-2 & -1.31\,E-2 & -1.06\,E-3 \\ -2.08\,E-1 & 2.44\,E-1 & -3.61\,E-2 & -3.41\,E-2 & -1.15\,E-1 \\ 2.89\,E-1 & -1.97\,E-1 & 1.68\,E-2 & 4.19\,E-2 & 8.32\,E-2 \end{bmatrix}$$

Model Matrices: C & D

$$C = \begin{bmatrix} 0 & 0 & 1 & 0 & 0 & 0 & 0 & 0 & 0 \\ 0 & 0 & 0 & 0 & 0 & 1 & 0 & 0 & 0 \\ 0 & 0 & 0 & 0 & 0 & 0 & 0 & 0 & 1 \end{bmatrix}$$

$$D = \begin{bmatrix} 2.10\,E-1 & -4.05\,E-1 & 3.39\,E-2 & -3.89\,E-3 & -1.44\,E-1 \\ 2.90\,E-2 & -7.26\,E-2 & -5.93\,E-2 & -1.16\,E-3 & -4.53\,E-2 \\ 6.80\,E-3 & -9.45\,E-2 & 1.77\,E-3 & 1.49\,E-2 & 4.69\,E-2 \end{bmatrix}$$

UIO Design (Example)

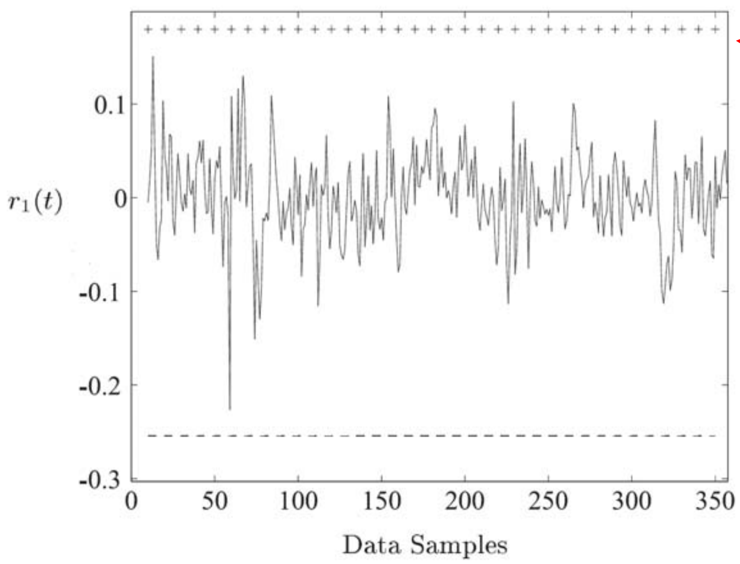

Fault detection thresholds with 10% margin

UIO eigenvalues near to 0.2

Fig. 5.36. The fault–free residual function $r_1(t)$ of the UIO driven by the O_s signal with minimum positive ('+') and negative ('-') thresholds.

UIO Design (Example, Cont'd)

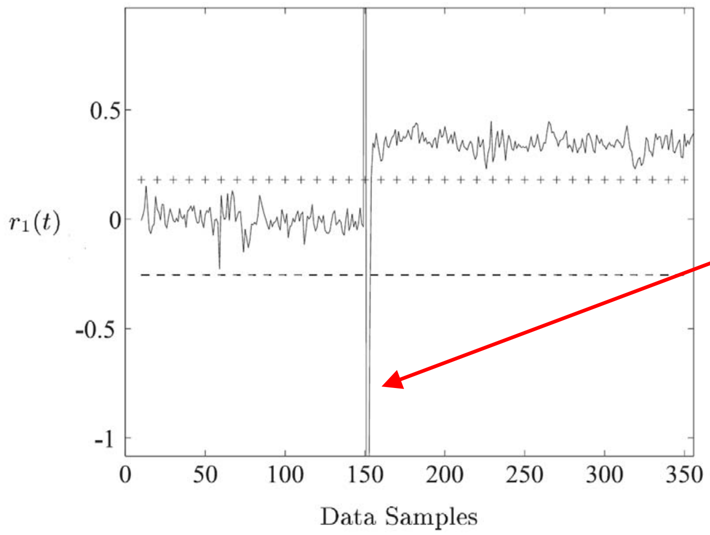

Input sensor fault at t=150 s.

Fig. 5.37. Residual function $r_1(t)$ of the UIO driven by the O_s signal in the presence of a fault.

OO Design (Example)

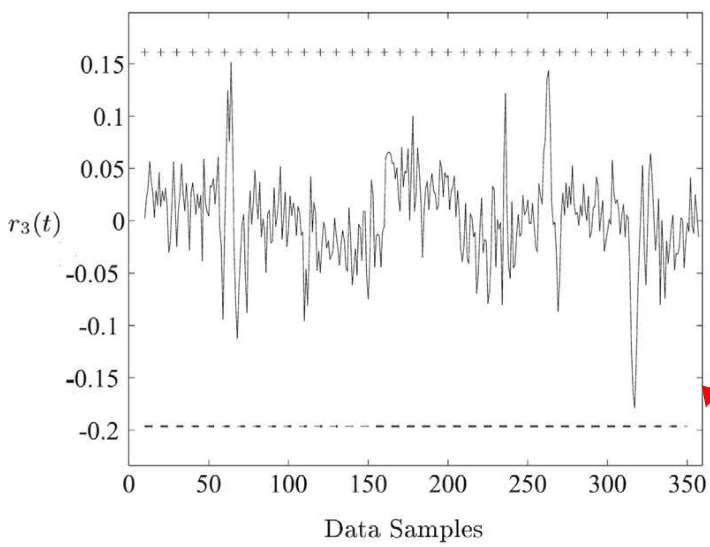

Fault detection thresholds with 10% margin.

OO eigenvalues between 0 and 0.2

Fig. 5.38. The fault–free residual function $r_3(t)$ of output observer driven by T_{rs} signal with minimum positive ('+') and negative ('-') thresholds.

OO Design (Example, Cont'd)

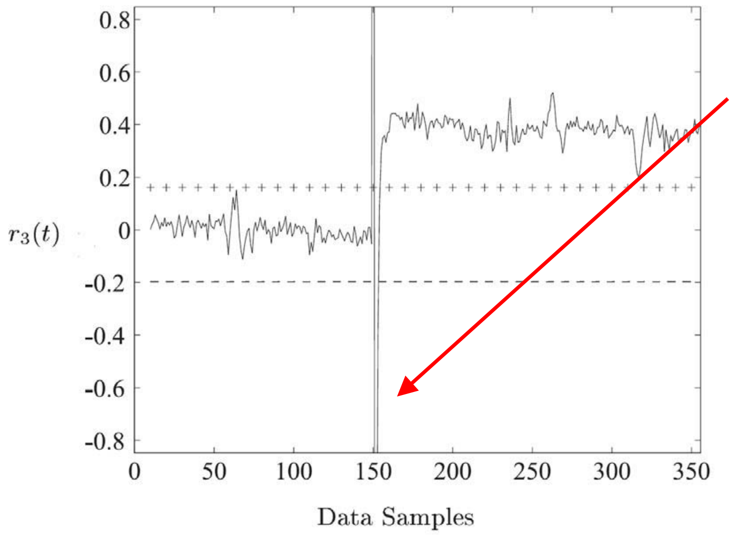

Output sensor fault commencing at *t=150s*.

Fault size 10% of the mean value of the corresponding output

Fig. 5.39. The residual function $r_3(t)$ of output observer driven by T_{rs} signal with a fault.

Minimal Detectable Faults

- OO and UIO
- Minimal fault sizes determined by trial and error procedure (simulations)

Table 5.14. Minimal detectable step and ramp faults with classical observers and UIO.

Sensor	C_b	O_s	Q_d	R_y	Q_a	P_v	T_s	T_{rs}
Step	30%	25%	20%	40%	45%	15%	5%	10%
Ramp	40%	30%	35%	55%	50%	40%	20%	30%

Kalman Filter FDI

- Kalman filter noise terms

Table 5.15. The three output estimation errors with equation error models.

Output	P_v	T_s	T_{rs}
Equation error	0.0146	0.0273	0.0051

- Minimal detectable faults

Table 5.16. Minimal detectable step and ramp faults with classical KF and UIKF.

Sensor	C_b	O_s	Q_d	R_y	Q_a	P_v	T_s	T_{rs}
Step	25%	15%	12%	35%	35%	10%	3%	5%
Ramp	35%	20%	20%	45%	40%	30%	5%	8%

Gas Turbine FDI (*3*)

- MIMO SIMULINK prototype of a real single-shaft industrial gas turbine

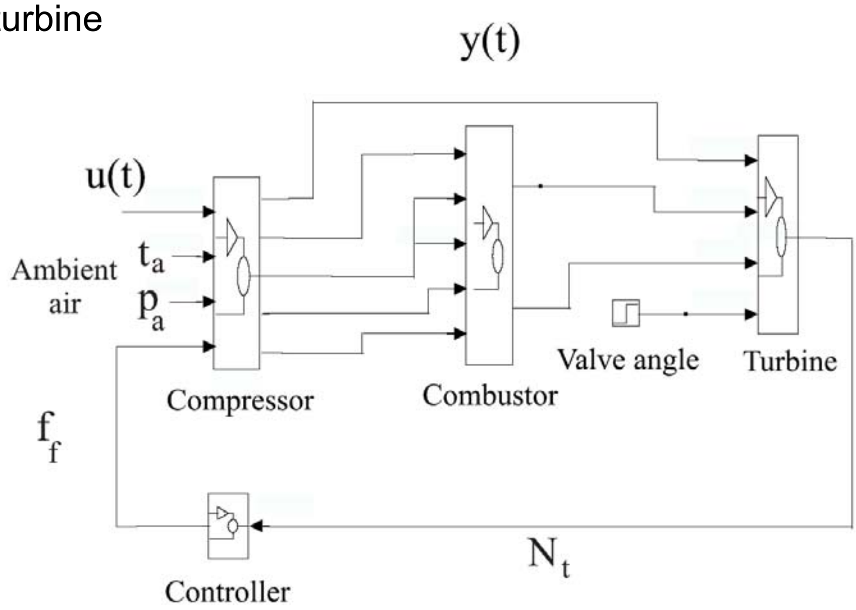

Turbine Control Inputs

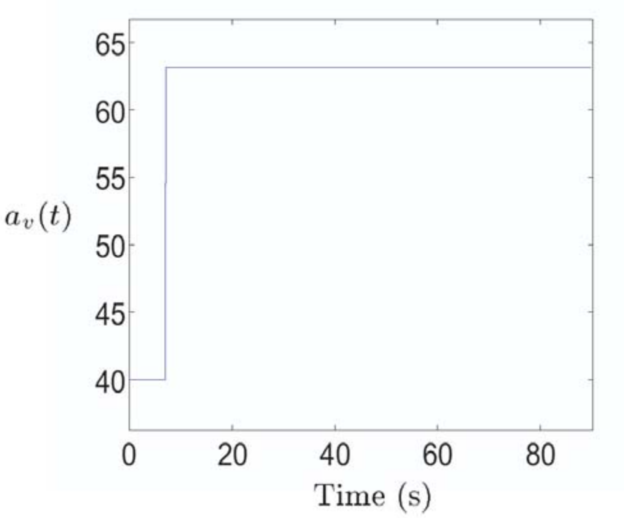

(a) $u_1(t) = a_v(t)$

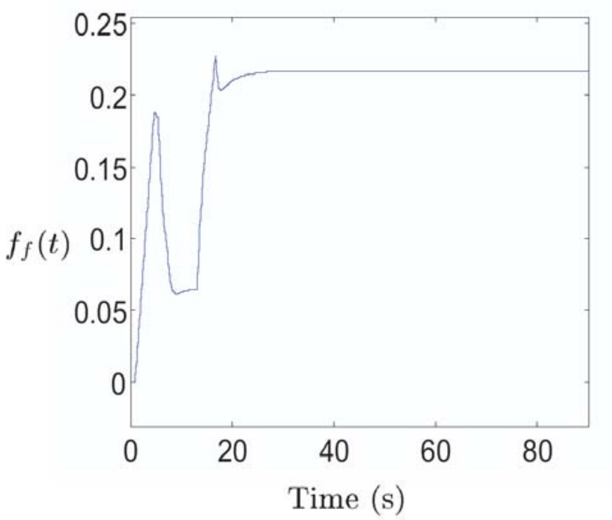

(b) $u_2(t) = f_f(t)$

Gas turbine input signals: (a) valve angle and (b) fuel flow

Turbine Block Diagram

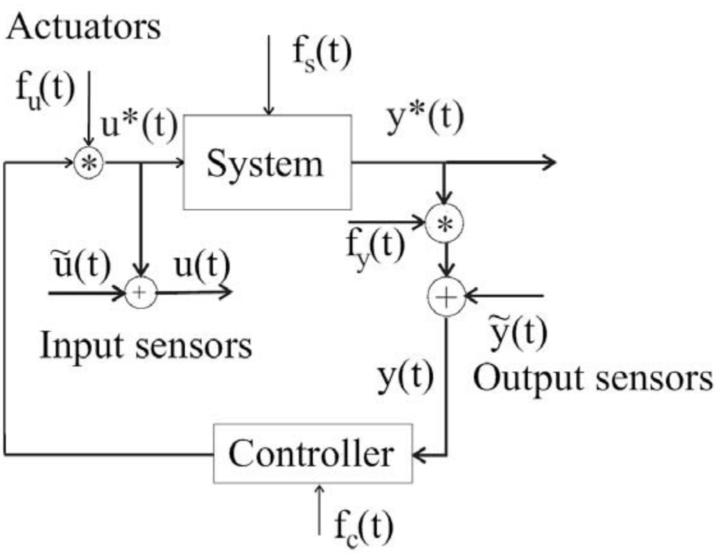

Fig. 5.46. Turbine closed–loop scheme.

Turbine Signal Details

- Turbine input accuracy

Table 5.24. Dynamic model identification: turbine inputs.

Variable	Name	Accuracy
t_a	amb. air temp.	$\pm 0.4^oC$
p_a	amb. air press.	$\pm 1\%$
f_f	fuel flow	$\pm 5\%$
a_v	valve angle	$\pm 2\%$

- Model identification

Table 5.25. Turbine output signals and MISO ARX model characteristics.

Variable label	Variable name	Model order	SSE	Accuracy
m_j	mass flow	2	$< 10^{-3}$	$\pm 5\%$
p_h	pressure	2	$< 10^{-4}$	$\pm 1\%$
q_l	torque	2	$< 10^{-4}$	$\pm 5\%$
t_k	temperature	2	$< 10^{-4}$	$\pm 1.5^oC$
w_t	speed	2	$< 10^{-5}$	$\pm 1\%$

Model Validation

Table 5.26. Dynamic ARX model validation.

Variable	Model order	SSE identif.	SSE 1st valid.	SSE 2nd valid.
m_j	2	$< 10^{-3}$	$< 10^{-3}$	< 0.01
p_h	2	$< 10^{-4}$	$< 10^{-3}$	< 0.01
q_l	2	$< 10^{-4}$	$< 10^{-3}$	< 0.1
t_k	2	$< 10^{-4}$	$< 10^{-3}$	< 0.1
w_t	2	$< 10^{-5}$	$< 10^{-5}$	< 0.1

- Estimation errors (loss function)

Variable	Name	Model order	$J(\theta)$	Accuracy
p_{h*}	Pressure	2	0.0054	$\pm$ 1%
m_{j*}	Mass flow	2	0.0049	$\pm$ 5%
q_{l*}	Torque	2	0.0042	$\pm$ 5%
t_{k*}	Temperature	2	0.0031	1.5^o

Model Parameters

Identified parameters, and input-output variance values

Variable	Model parameters θ	
p_{h*}	$[-0.0295,\ 1.0054,\ 0.1369,\ -0.1328,\ 0.0402,\ -0.0232]$	
m_{j*}	$[0.6655,\ 0.2885,\ -0.0579,\ 0.0651,\ 0.2408,\ -0.2065]$	
q_{l*}	$[-0.9920,\ 1.9904,\ -0.0179,\ 0.0181,\ 0.0111,\ -0.0100]$	
t_{k*}	$[-1.1760,\ 2.1882,\ 0.0283,\ -0.0311,\ -0.3202,\ 0.3133]$	
Variable	Input noises $\tilde{\sigma}_u$	Output noise $\tilde{\sigma}_y$
p_{h*}	$[0.0004,\ 0.0023]$	0.0026
m_{j*}	$[0.0004,\ 0.0023]$	0.0026
q_{l*}	$[0.0004,\ 0.0023]$	0.0015
t_{k*}	$[0.0004,\ 0.0023]$	0.0024

Fault Cases (Fault *Case 1*)

- Fault **case 1** represents fouling of the surfaces of the compressor blades, this reduces air flow, changes the blade aerodynamics and consequently changes the surface roughness
- The failure is modelled as a gradual decrease in mass flow rate for a given pressure ratio
- The maximum decrease in mass flow rate is set nominally at 5%
- Fault development rate is set to (5% decrease of normal flow rate)/hour.

FDI Scheme (Fault *Case 1*)

- Submodel

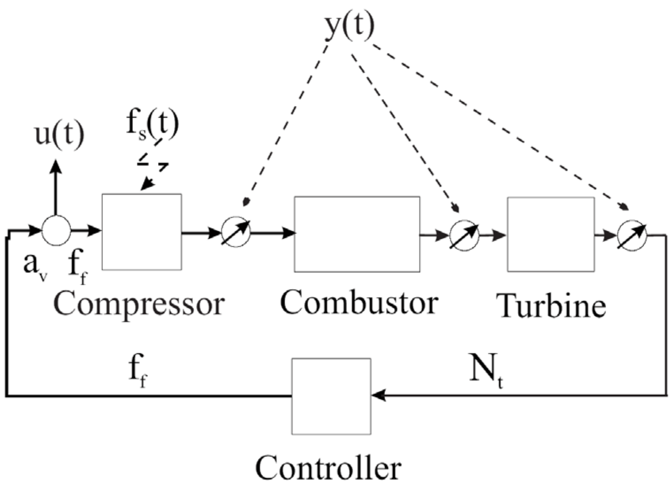

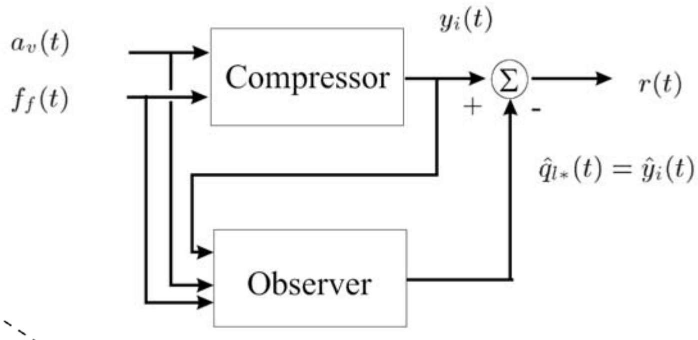

- Output observer for fault detection

Fault *Case 1* Signals

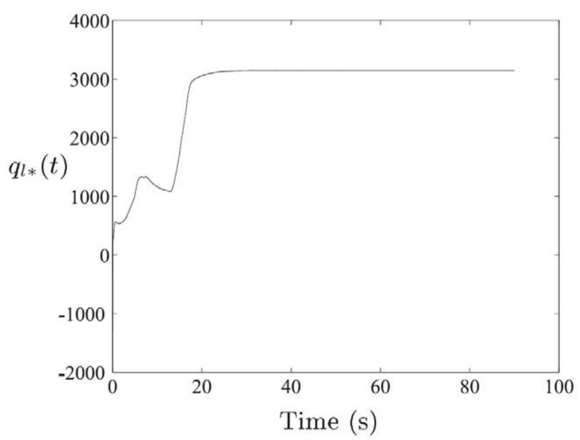

(a) $q_{l*}(t)$ output

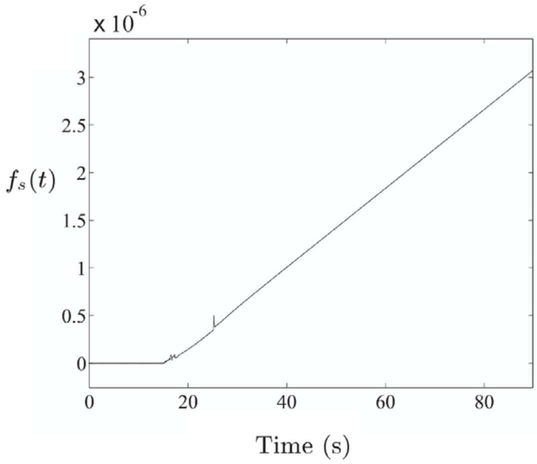

(b) The simulated fault $f_s(t)$

Fault *Case 1* Detection

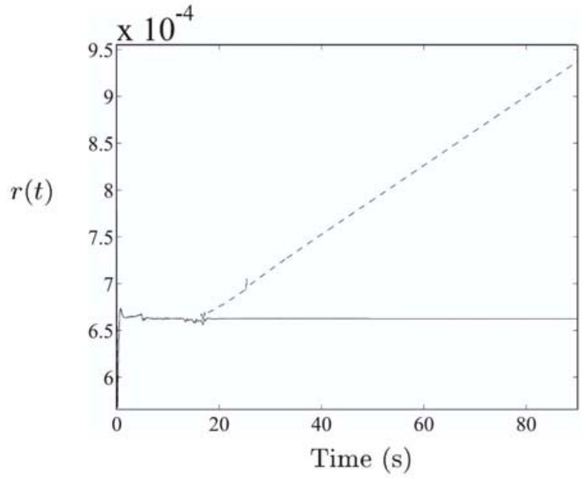

(b) Fault-free (solid line) and faulty (dashed line) residual $r(t)$

Observer eigenvalues near to 0.3

Ramp fault case

Fault starts at *t=15s.*

Fig. 5.51. Results from the residual generation.

Fault Cases (Fault *Case 2*)

- The **case 2** fault represents the malfunctioning of a thermocouple in the turbine gas
- It leads to a slowly increasing or decreasing reading over time
- There is no limit placed on the error magnitude
- The fault development rate is set to (5% error in measuring actual temperature)/hour

Fault *Case 2* Detection

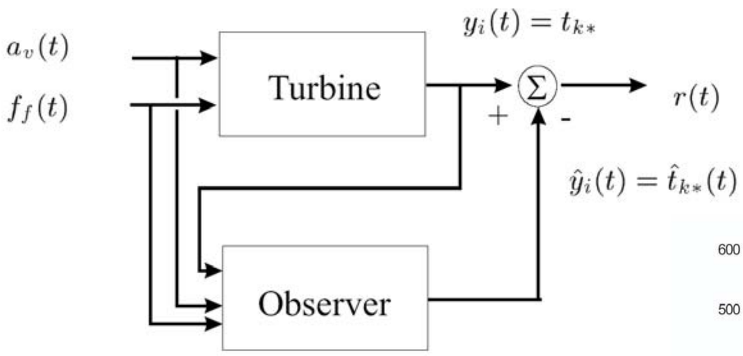

- Output observer structure and diagnostic signal

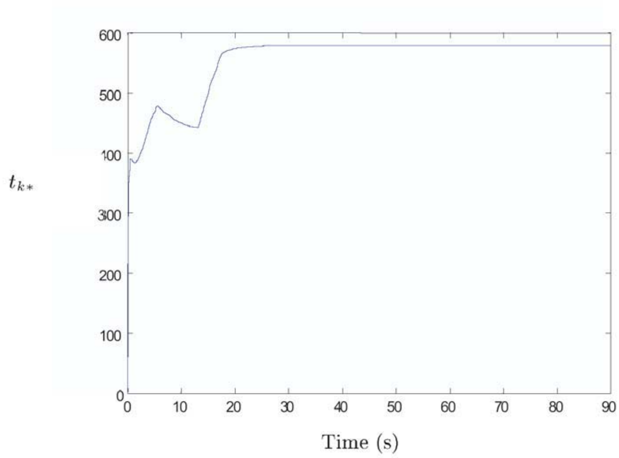

- Observer eigenvalues chosen near to 0.3

Fault *Case 2* Signals

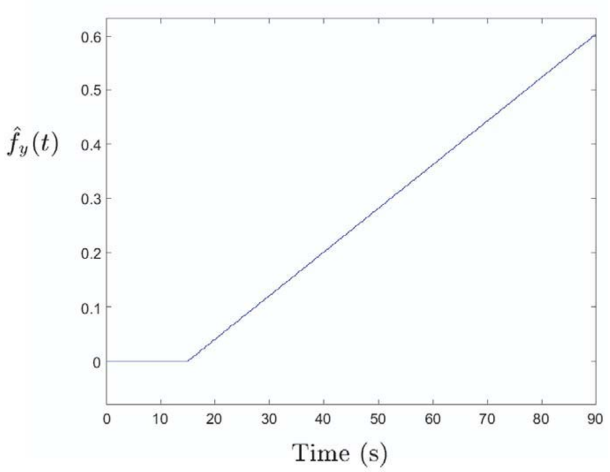

(a) Measured fault function

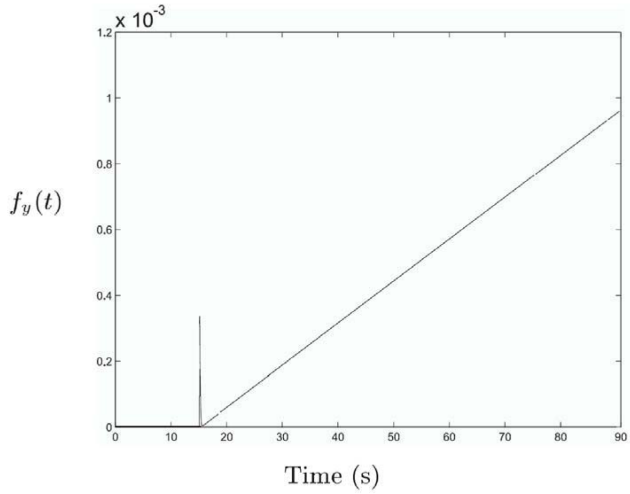

(b) Estimated fault signal

Real and estimated fault signals

Fault *Case 2* Results

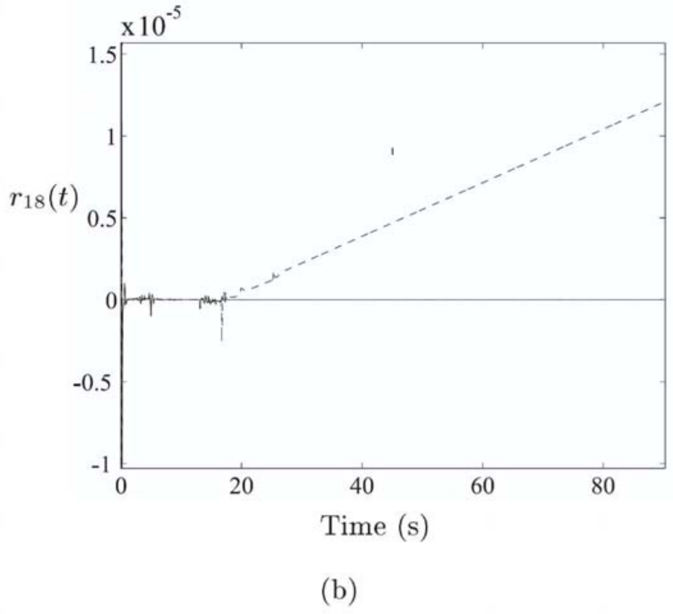

Fig. 5.54. Residual function in different operating points.

Fault Cases (Fault *Case 3*)

- Fault **case 3** represents the fault $f_s(t)$ of the turbine
- This results in a reduction in turbine efficiency
- The fault is modelled as a gradual reduction in turbine efficiency over time
- The maximum decrease in turbine efficiency is set nominally at 5%
- Fault development rate is set to (5% reduction of normal efficiency)/hour

Fault *Case 3* Signals

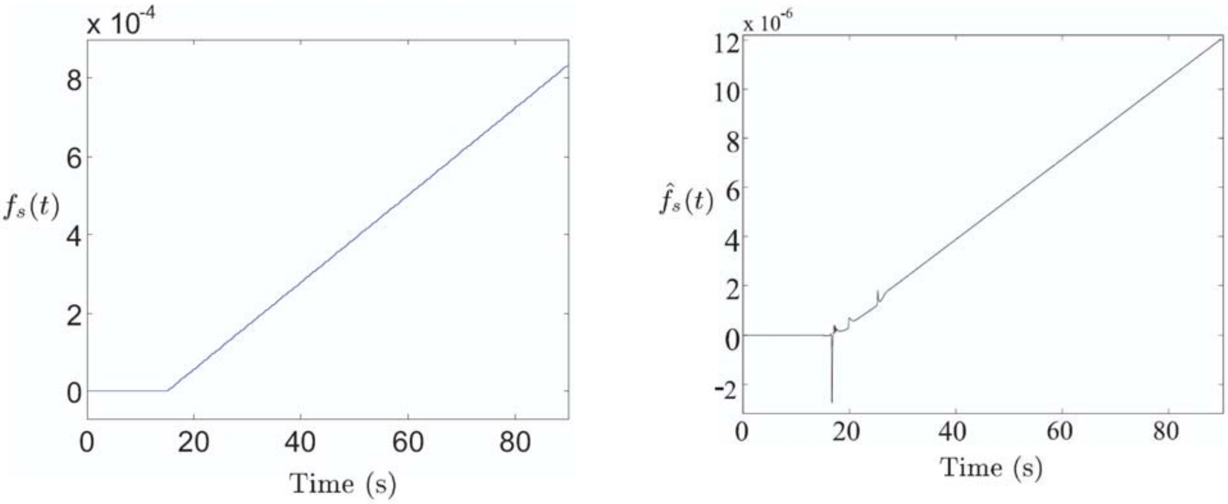

(a) Actual (b) Estimated

Real and estimated fault signals

Fault *Case 3* Detection

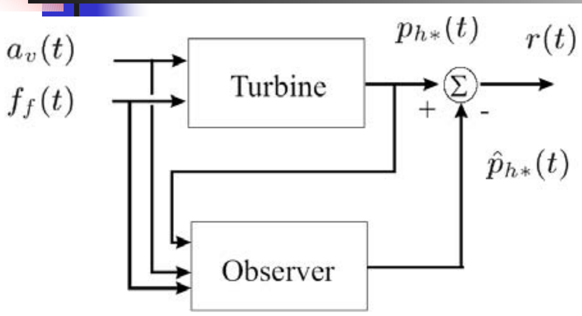

(a) $p_{h*}(t)$ residual generation scheme

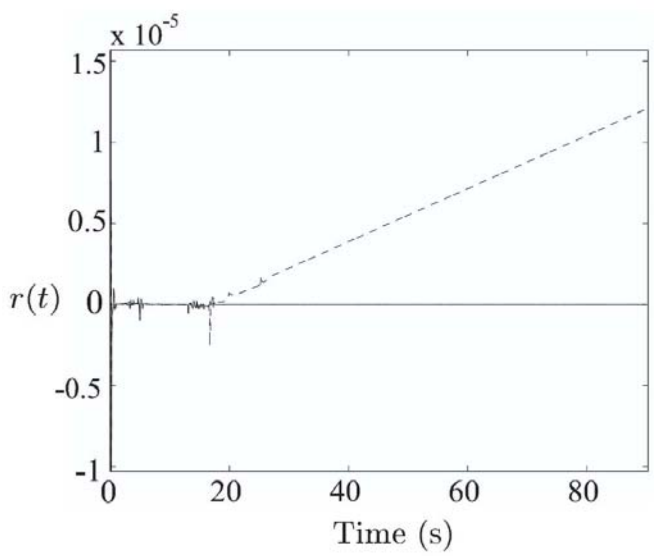

(b) $p_{h*}(t)$ observer residual

Residual generation strategy and diagnostic signal

Fault Cases (Fault *Case 4*)

- Fault **case 4** $f_c(t)$ affects the actuator of the turbine controller
- Under the assumption that there are no actuator dynamics in the current turbine model, the fault $f_c(t)$ of the actuator causes a slower response to demanded flow rates
- Its effect is modelled as a simple first order lag on the resulting fuel flow
- The actuator response time constant increases linearly with the time in order to represent a progressive damage to the actuator

Fault *Case 4* Detection

- FDI subsystem

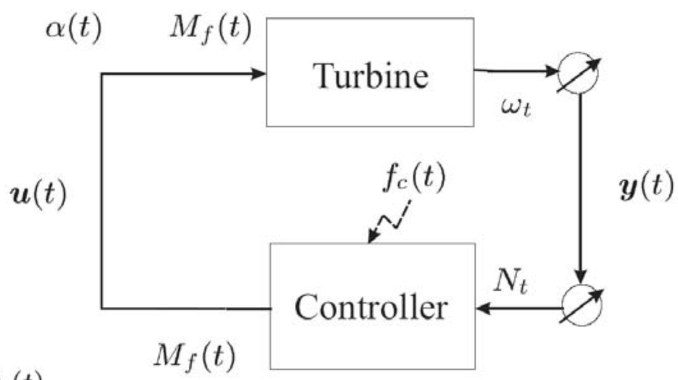

(a) The diagnosis subsystem

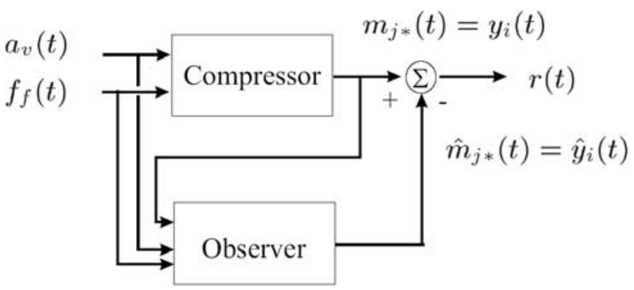

(b) The observer scheme

- Diagnosis observer (eigenvalues near 0.4)

Fault *Case 4* Signal Details

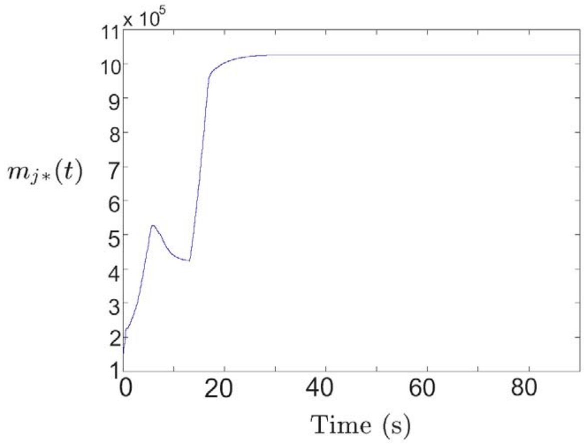

(a) The $m_{j*}(t)$ turbine mass flow signal.

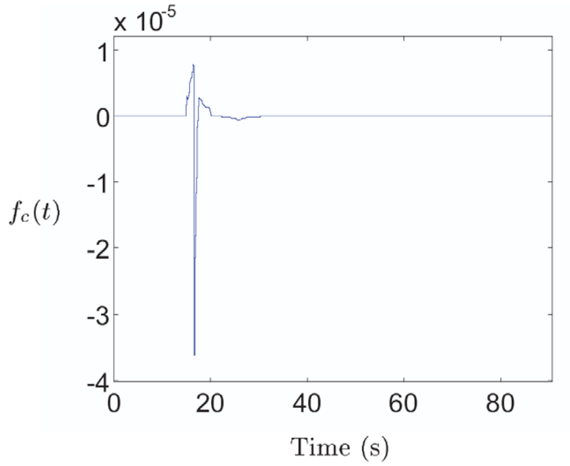

(b) The fault $f_c(t)$ concerning $m_{j*}(t)$

Monitored output signal and fault mode

Fault *Case 4* Signal Details

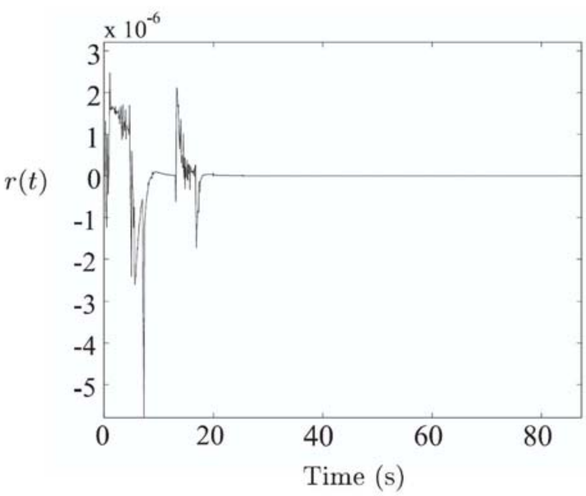

(a) Fault-free residual

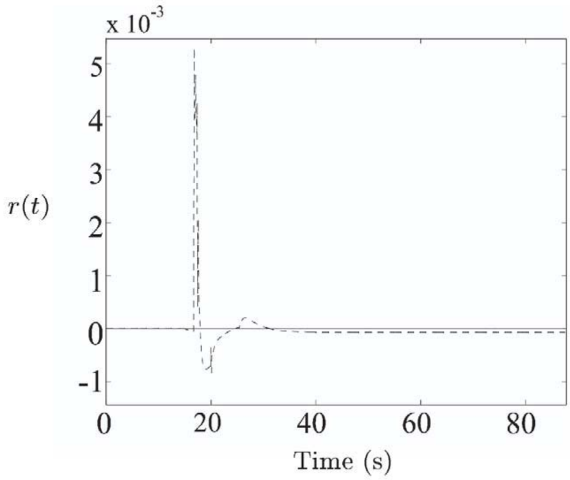

(b) Residual in the presence of $f_c(t)$ fault

- Fault commences at *t=15s.*

Fault Isolation

- Each fault affects a different output (FMEA…)
  - Failure Mode and Effect Analysis
  - Engineering procedure
  - Fault effects on each output: sensitivity analysis
- One observer for each output
- **Fault signature**

Fault/$r(t)$	q_{l*}	t_{k*}	p_{h*}	m_{j*}
Case 1	1	0	0	0
Case 2	0	1	0	0
Case 3	0	0	1	0
Case 4	0	0	0	1

Kalman Filter Design

Identified parameters, and input-output variance values

Variable	Model parameters θ
p_{h*}	$[-0.0295,\ 1.0054,\ 0.1369,\ -0.1328,\ 0.0402,\ -0.0232]$
m_{j*}	$[0.6655,\ 0.2885,\ -0.0579,\ 0.0651,\ 0.2408,\ -0.2065]$
q_{l*}	$[-0.9920,\ 1.9904,\ -0.0179,\ 0.0181,\ 0.0111,\ -0.0100]$
t_{k*}	$[-1.1760,\ 2.1882,\ 0.0283,\ -0.0311,\ -0.3202,\ 0.3133]$

Variable	Input noises $\tilde{\sigma}_u$	Output noise $\tilde{\sigma}_y$
p_{h*}	$[0.0004,\ 0.0023]$	0.0026
m_{j*}	$[0.0004,\ 0.0023]$	0.0026
q_{l*}	$[0.0004,\ 0.0023]$	0.0015
t_{k*}	$[0.0004,\ 0.0023]$	0.0024

FDI with KF: Fault *Case 1*

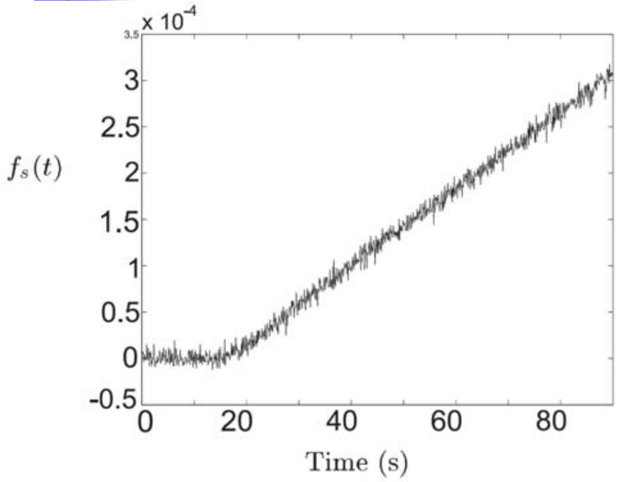

(a) System fault $f_s(t)$

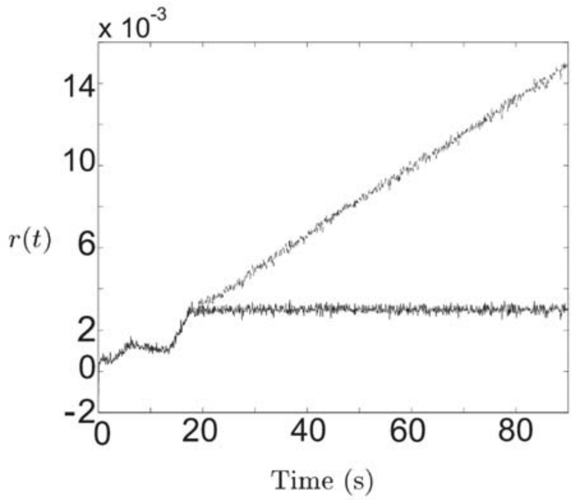

(b) Kalman filter residuals in fault–free (black line) and faulty (gray line) cases.

- Fault @ *t=15s.*

FDI with KF: Fault *Case 2*

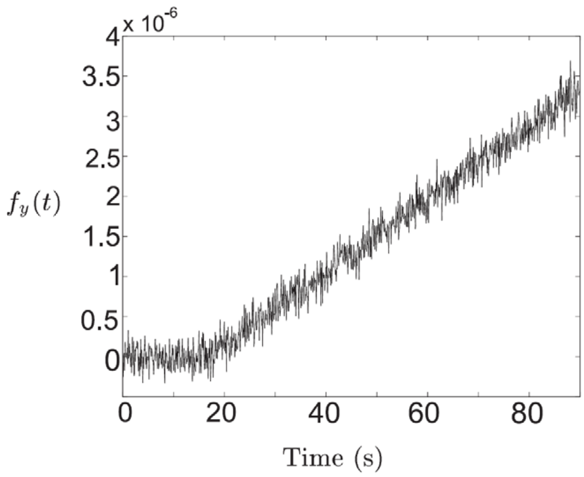

(a) Output sensor fault $f_y(t)$

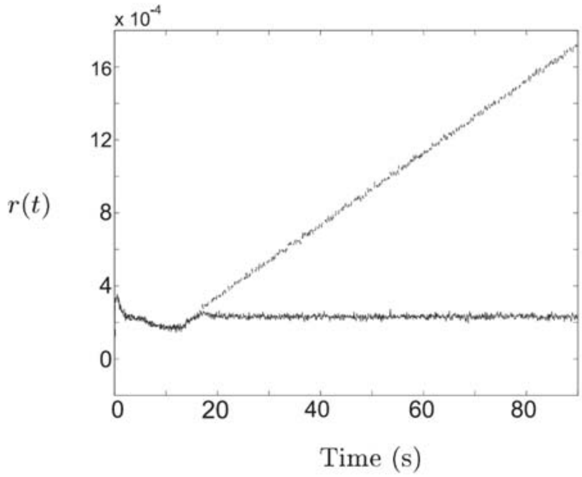

(b) Kalman filter residuals in fault–free (black line) and faulty (gray line) cases.

- Fault @ *t=15s.*

FDI with KF: Fault *Case 3*

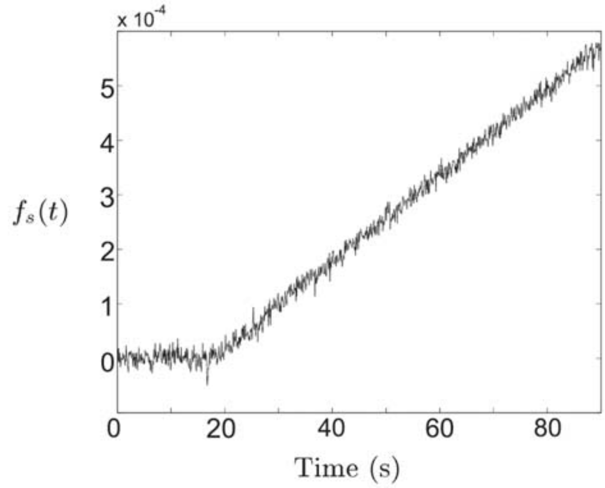

(a) System fault $f_s(t)$

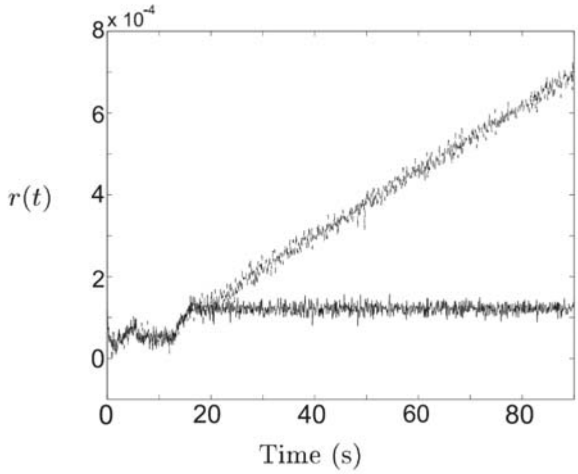

(b) Kalman filter residuals in fault–free (black line) and faulty (gray line) cases.

- Fault @ *t=15s.*

FDI with KF: Fault *Case 4*

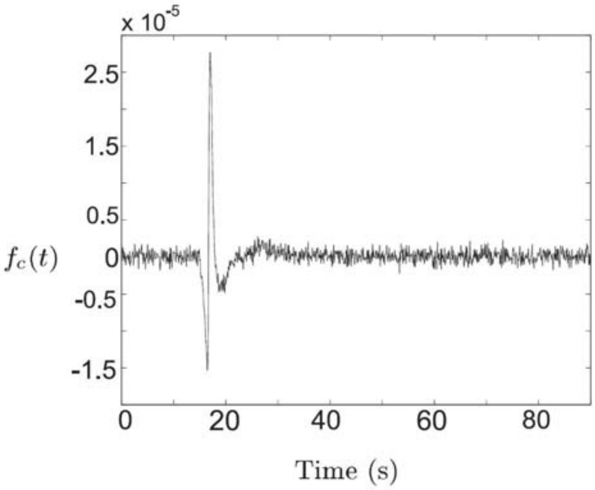

(a) Actuator fault $f_c(t)$

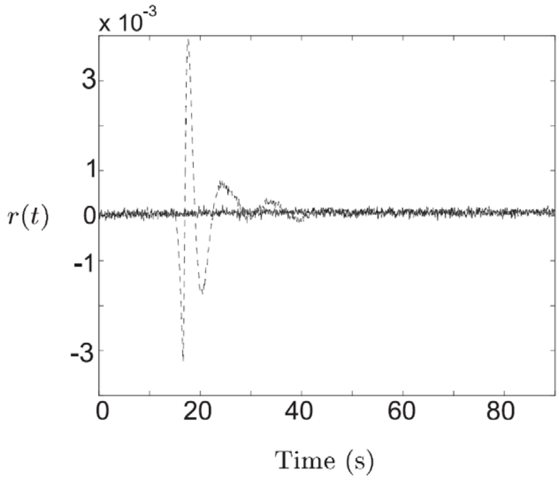

(b) Kalman filter residual

- Fault @ *t=15s.* but different dynamics

Minimal Detectable Faults

- Ramp functions
- A detection delay is defined
- Positive and negative thresholds

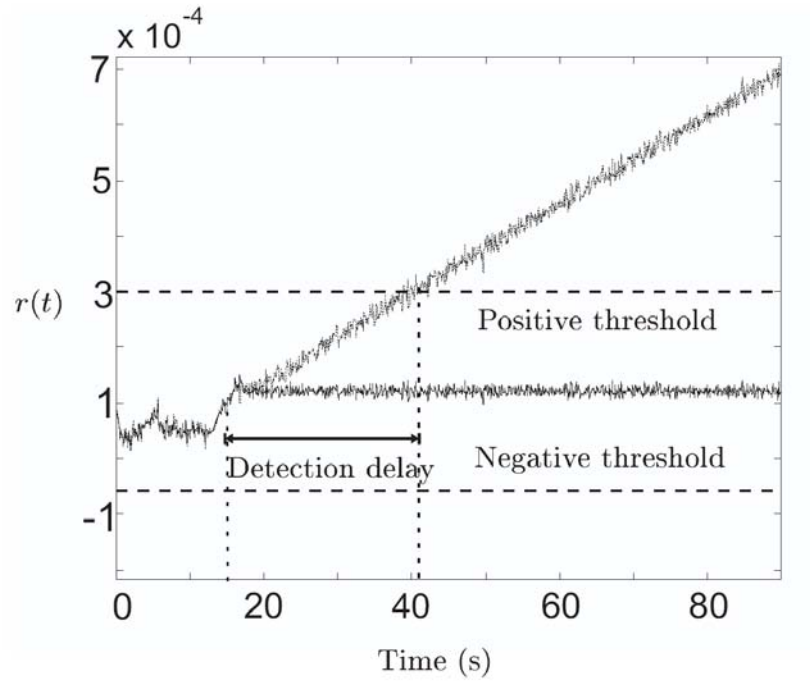

Minimal Detectable Faults (Cont'd)

Fault Case	Monitored signal	Noise free	Noisy case	Detection delay
Case 1 (Compressor fault)	$q_{l*}(t)$	0.5%	1%	30s
Case 2 (Thermocouple sensor fault)	$t_{k*}(t)$	10%	12%	30s
Case 3 (Turbine failure)	$p_{h*}(t)$	5%	7%	60s
Case 4 (Actuator fault)	$m_{j*}(t)$	1%	3%	10s

Minimum detectable faults by monitoring residual and innovation values

Small Aircraft FDI (*4*)

- Aircraft axes and angles

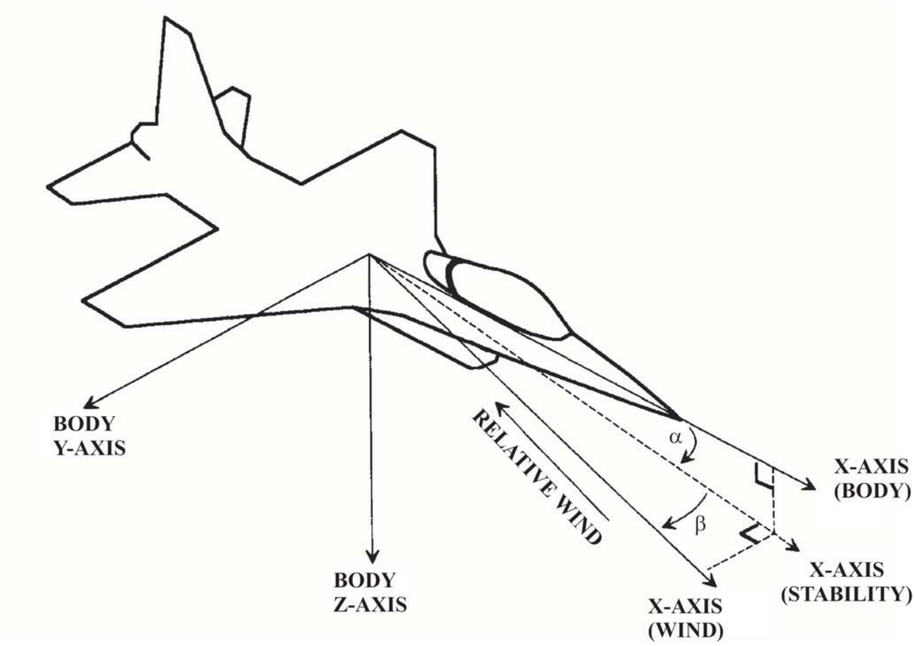

Aircraft Nonlinear Model

- Aircraft nonlinear simplified model
- 4 inputs and 10 outputs
- 3 disturbance signals

$$
\begin{aligned}
\dot{V} &= -\frac{(C_{D0} + C_{D\alpha}\alpha + C_{D\alpha_2}\alpha^2)}{m}V^2 + g\,(\sin\alpha\cos\theta\cos\phi - \cos\alpha\sin\theta) \\
&\quad + \frac{\cos\alpha}{m}\frac{t_p}{V}\,(t_0 + t_1 n_e)\,\delta_{th} + w_v\sin\alpha \\
\dot{\alpha} &= -\frac{(C_{L0} + C_{L\alpha}\alpha)}{m}V + \frac{g}{V}\,(\cos\alpha\cos\theta\cos\phi + \sin\alpha\sin\theta) + q_\omega \\
&\quad - \frac{\sin\alpha}{m}\frac{t_p}{V^2}\,(t_0 + t_1 n_e)\,\delta_{th} + \frac{\cos\alpha}{V}w_v \\
\dot{\beta} &= \frac{(C_{D0} + C_{D\alpha}\alpha + C_{D\alpha_2}\alpha^2)\sin\beta + C_{Y\,\beta}\beta\cos\beta}{m}V + g\frac{\cos\theta\sin\phi}{V} \\
&\quad + p_\omega\sin\alpha - r_\omega\cos\alpha - \frac{\cos\alpha\sin\beta}{m}\frac{t_p}{V^2}\,(t_0 + t_1 n_e)\,\delta_{th} + \frac{1}{V}w_\ell \\
\dot{p}_\omega &= \frac{(C_{l\beta}\beta + C_{lp}\,p_\omega)}{I_x}V^2 + \frac{(I_y - I_z)}{I_x}\,q_\omega r_\omega + \frac{C_{\delta_a}}{I_x}V^2\delta_a \\
\dot{q}_\omega &= \frac{(C_{m0} + C_{m\alpha}\alpha + C_{mq}\,q_\omega)}{I_y}V^2 + \frac{(I_z - I_x)}{I_y}\,p_\omega r_\omega + \frac{C_{\delta_e}}{I_y}V^2\delta_e \\
&\quad + \frac{t_d}{I_y}\frac{t_p}{V}\,(t_0 + t_1 n_e)\,\delta_{th} \\
\dot{r}_\omega &= \frac{(C_{n\beta}\beta + C_{nr}\,r_\omega)}{I_z}V^2 + \frac{(I_x - I_y)}{I_z}\,p_\omega q_\omega + \frac{C_{\delta_r}}{I_z}V^2\delta_r \\
\dot{\phi} &= p_\omega + (q_\omega\sin\phi + r_\omega\cos\phi)\tan\theta \\
\dot{\theta} &= q_\omega\cos\phi - r_\omega\sin\phi \\
\dot{\psi} &= \frac{(q_\omega\sin\phi + r_\omega\cos\phi)}{\cos\theta} \\
\dot{n}_e &= t_n n_e^3 + \frac{t_f}{n_e}\,(t_0 + t_1 n_e)\,\delta_{th}
\end{aligned}
$$

Navigation and Guidance System

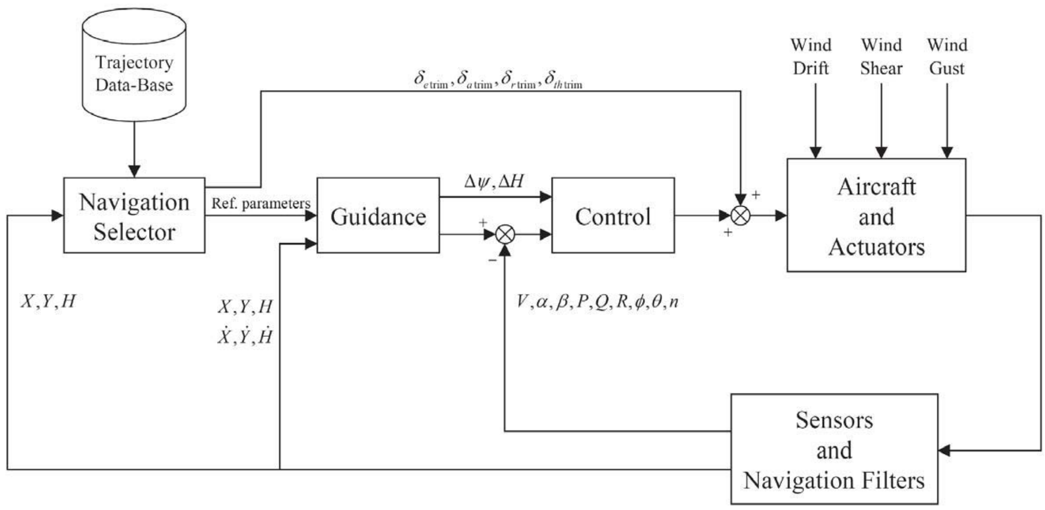

Overall architecture of the NGC system

Linear Identified Model

$$\dot{x}(t) = A\,x(t) + B\,c(t) + E\,d(t)$$

- State-space model, with:

$$x(t) = [\ \Delta V(t) \quad \Delta\alpha(t) \quad \Delta\beta(t) \quad \Delta p_\omega(t) \quad \Delta q_\omega(t) \quad \Delta r_\omega(t)$$
$$\dots \quad \Delta\phi(t) \quad \Delta\theta(t) \quad \Delta\psi(t) \quad \Delta H(t) \quad \Delta n_e(t)\ ]^{\mathrm{T}}$$
$$c(t) = [\ \Delta\delta_e(t) \quad \Delta\delta_a(t) \quad \Delta\delta_r(t) \quad \Delta\delta_{th}(t)\ ]^{\mathrm{T}}$$
$$d(t) = [\ w_u(t) \quad w_v(t) \quad w_w(t)\ ]^{\mathrm{T}}$$

Input Signals and Noise

- Input sensor errors parameters

Input sensor	Bias	White Noise Std
Elevator deflection angle	0.0052 rad	0.0053 rad
Aileron deflection angle	0.0052 rad	0.0053 rad
Rudder deflection angle	0.0052 rad	0.0053 rad
Throttle aperture	1%	1%

- Wind gust parameters

Correlation time	Wind covariance
$\tau_u = 2.326\,\mathrm{s}$	$E[w_u^2] = 0.7\,(\mathrm{m/s})^2$
$\tau_v = 7.143\,\mathrm{s}$	$E[w_v^2] = 0.7\,(\mathrm{m/s})^2$
$\tau_w = 0.943\,\mathrm{s}$	$E[w_w^2] = 0.7\,(\mathrm{m/s})^2$

Identification/Validation Data

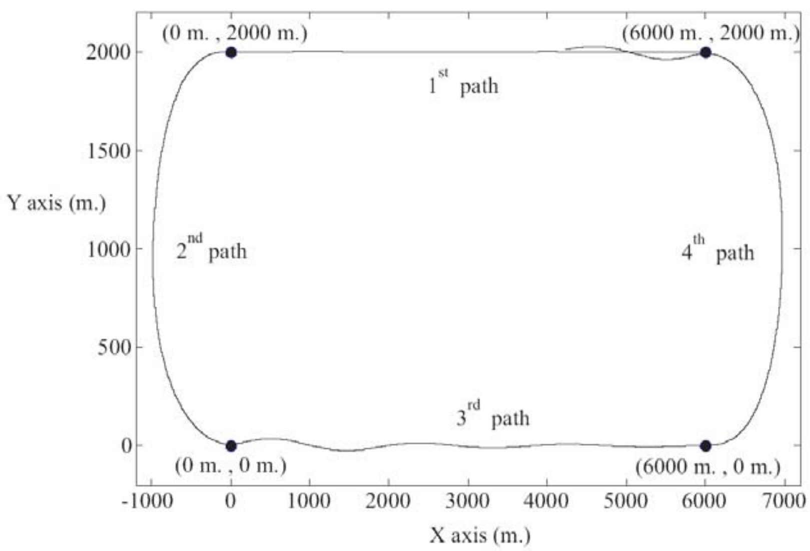

Figure 6.7: Aircraft complete trajectory example.

State-Space Matrices

- **Model order** n=10 - 11
- **Aircraft model matrix** A

$$A = \begin{bmatrix} -0.0458 & -0.1856 & 0 & -9.8025 & 0 & 2.4626 & 0 & 0 & -0.2460 & 0 & 0.0004 \\ -0.0054 & -1.4808 & 0.9399 & 0.0012 & 0 & 0.0007 & 0.0062 & 0.0005 & -0.0472 & 0 & 0 \\ 0.0229 & -12.1598 & -7.9809 & -0.0036 & 0 & -0.0014 & 0.0249 & -0.0006 & 0.1418 & 0 & 0 \\ 0 & 0 & 0.9688 & 0 & 0 & 0 & 0 & -0.2477 & -0.0499 & 0 & 0 \\ 0 & -48.4491 & 0 & 49.9842 & 0 & -12.3526 & 0 & 0 & 1.2544 & 0 & 0 \\ -0.0010 & 0.0001 & 0 & -0.0048 & 0 & -0.1412 & 0.0767 & -0.9971 & 0.1895 & 0 & 0 \\ 0 & 0 & -0.0450 & 0 & 0 & -6.3604 & -3.6226 & 0.5711 & 0 & 0 & 0 \\ 0 & 0 & -0.0024 & 0 & 0 & 2.9001 & -0.4618 & -0.6996 & 0 & 0 & 0 \\ 0 & 0 & 0.0181 & 0.0501 & 0 & 0 & 1.0000 & 0.0707 & 0 & 0 & 0 \\ 0 & 0 & 0.2484 & 0.0036 & 0 & 0 & 0 & 0.9714 & 0 & 0 & 0 \\ 0 & 0 & 0 & 0 & 0 & 0 & 0 & 0 & 0 & 0 & -0.4532 \end{bmatrix}$$

State-Space Matrices (Cont'd)

Aircraft model matrices B and E

$$B = \begin{bmatrix} 0 & 0.0009 & -0.0136 & 1.7473 \\ -0.3067 & 0 & 0 & -0.0026 \\ -40.6088 & 0 & 0 & -0.2459 \\ 0 & 0 & 0 & 0 \\ 0 & 0 & 0 & 0 \\ 0 & -0.0027 & 0.0427 & 0.0002 \\ 0 & -5.6695 & 1.0452 & 0 \\ 0 & -0.1215 & -2.4324 & 0 \\ 0 & 0 & 0 & 0 \\ 0 & 0 & 0 & 0 \\ 0 & 0 & 0 & 706.4263 \end{bmatrix}, \quad E = \begin{bmatrix} -0.0662 & 0.0496 & 0.1031 \\ -0.0662 & 0.0487 & 0.1031 \\ 0.2006 & -0.1460 & -0.6426 \\ 0 & 0 & 0 \\ 0.0727 & -0.2470 & -0.9663 \\ -0.0010 & -0.0028 & -0.0001 \\ -0.0005 & -0.1272 & -0.0035 \\ 0.0004 & 0.0580 & -0.0005 \\ 0 & 0 & 0 \\ 0 & 0 & 0 \\ 0 & 0 & 0 \end{bmatrix}$$

Minimal Detectable Faults (UIO)

- UIO: 4 residual generators (one for each input signal) de-coupled from 1 input sensor (fault)

Sensor $c_i(t)$	Var.	Fault Size	Delay
Elevator deflection angle	δ_e	2^o	18 s
Aileron deflection angle	δ_a	3^o	6 s
Rudder deflection angle	δ_r	4^o	8 s
Throttle aperture %	δ_{th}	2%	15 s

Minimal Detectable Faults (UIO, Cont'd)

- Bank residuals for the 1st control input fault isolation
- Optimised eigenvalues
- Thresholds fixed as fault-free residual mean ± 4*standard deviation values

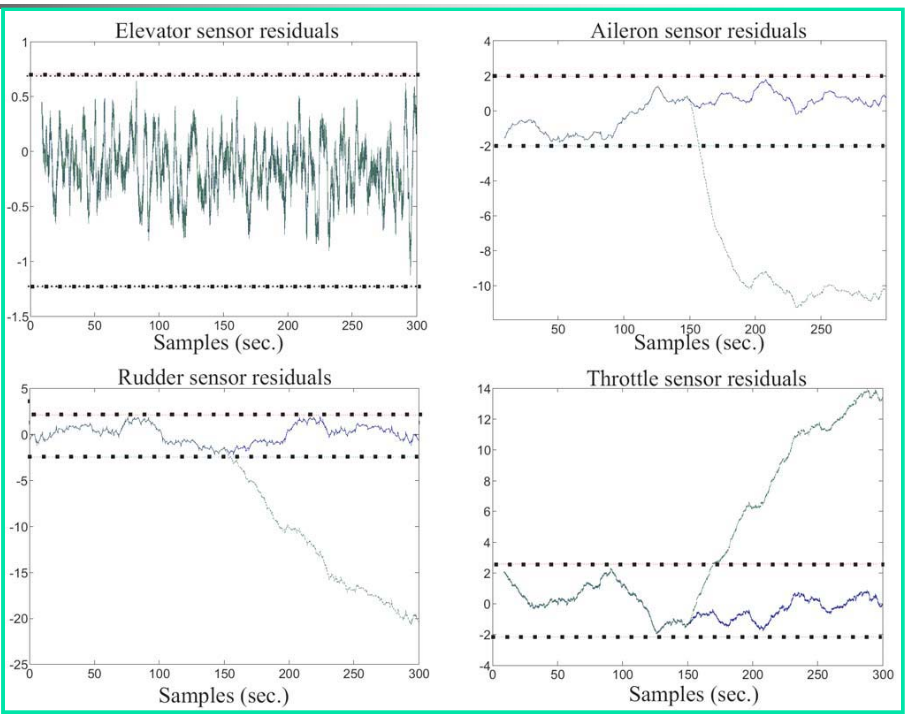

Minimal Detectable Faults (OO)

- OO: 9 MISO residual generators (one for each output)

Sensor $y_i(t)$	Var.	Fault Size	Delay
True Air Speed	V	8 m/s	9 s
Pitch Rate	q_ω	3^o/s	22 s
Elevation Angle	θ	5^o	10 s
Altitude	H	8 m	12 s
Roll Rate	p_ω	2^o/s	24 s
Yaw Rate	r_ω	3^o/s	29 s
Bank Angle	ϕ	5^o	5 s
Heading Angle	ψ	6^o	20 s
Engine Speed	n_e	20 rpm	25 s

Minimal Detectable Faults (OO, Cont'd)

- Bank residuals for the 9th output sensor fault isolation
- Optimised eigenvalues
- Thresholds fixed as fault-free residual mean ± 9*standard deviation values

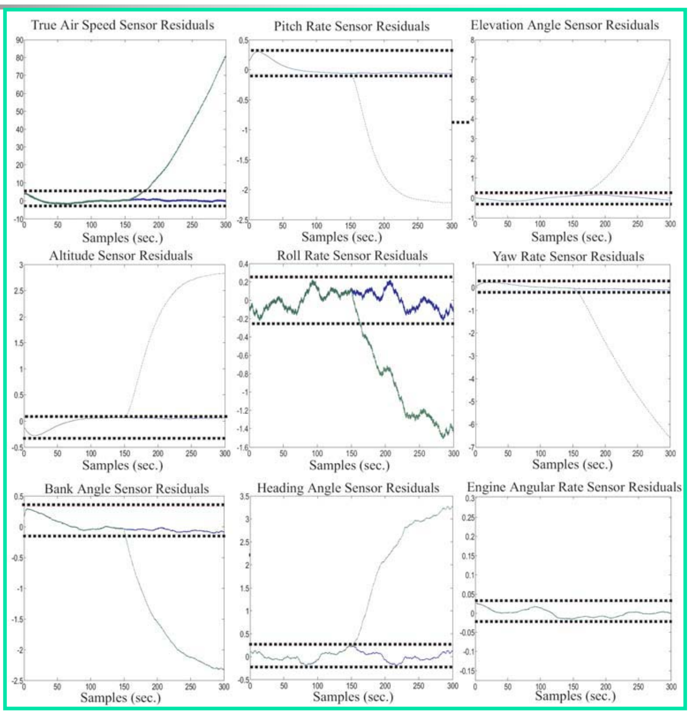

Kalman Filter for FDI

- KF residuals vs. OO residuals

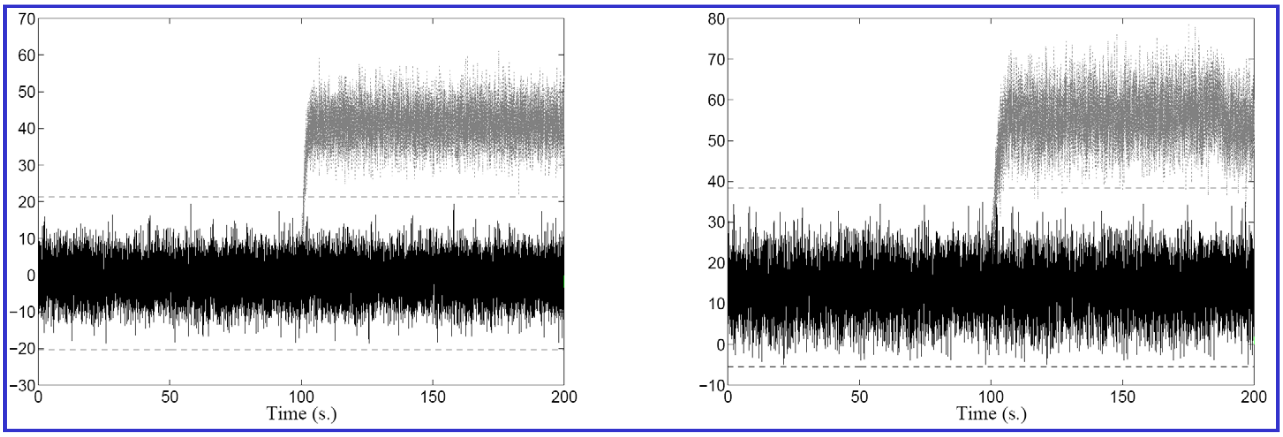

- Smaller minimal detectable faults

Satellite FDI (*5*)

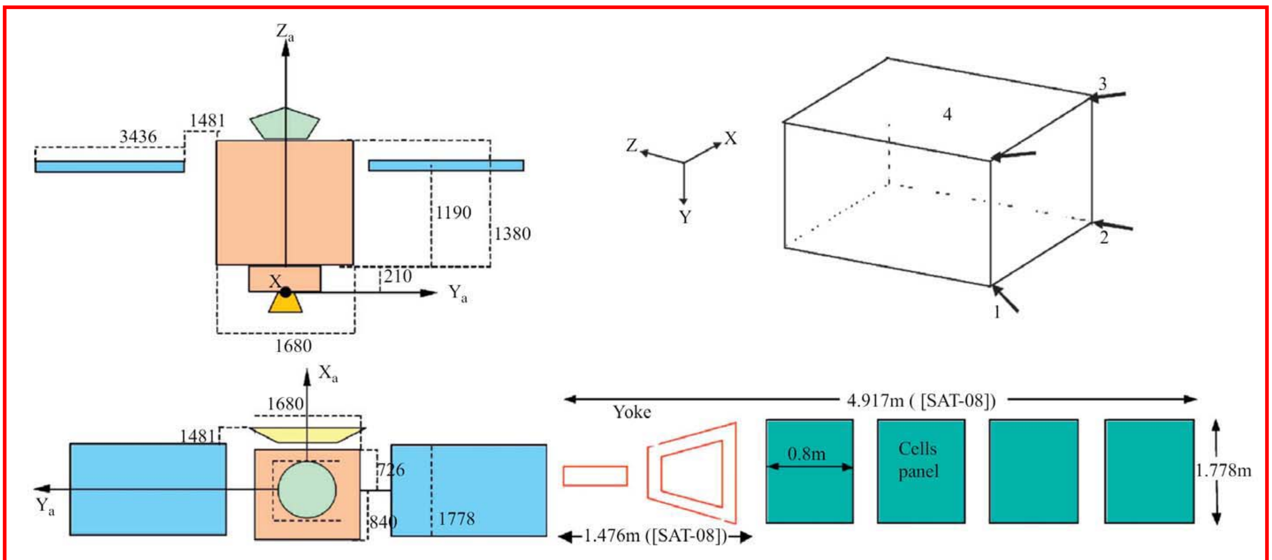

Fig. 1. The MEX structure.

Satellite Structure

- Redundant configuration of 4 thrusters
- 2 IMUs (Inertial Measurement Unit)
- Satellite dynamic model

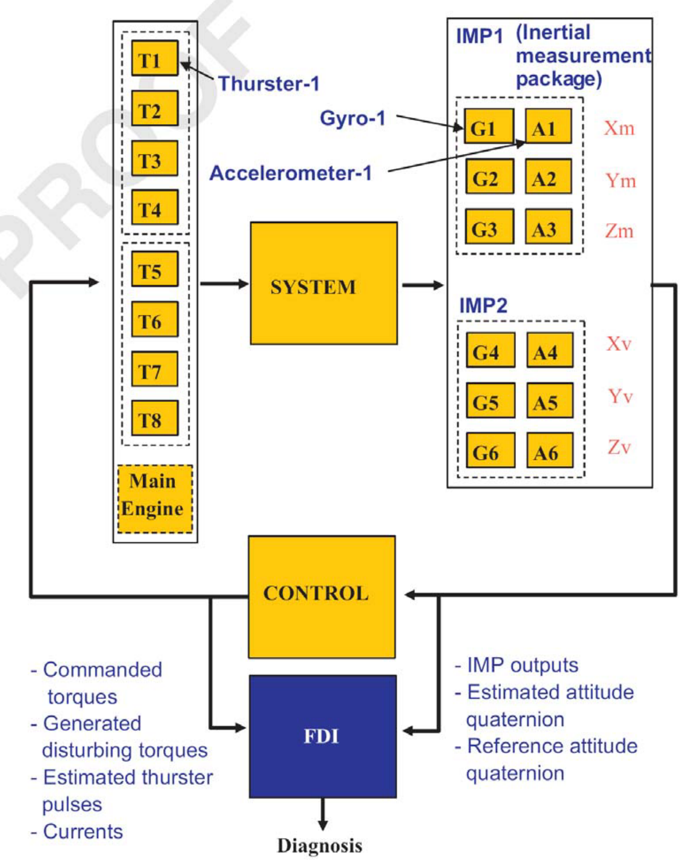

Fig. 2. MEX IMU and thruster configurations.

Satellite Control System

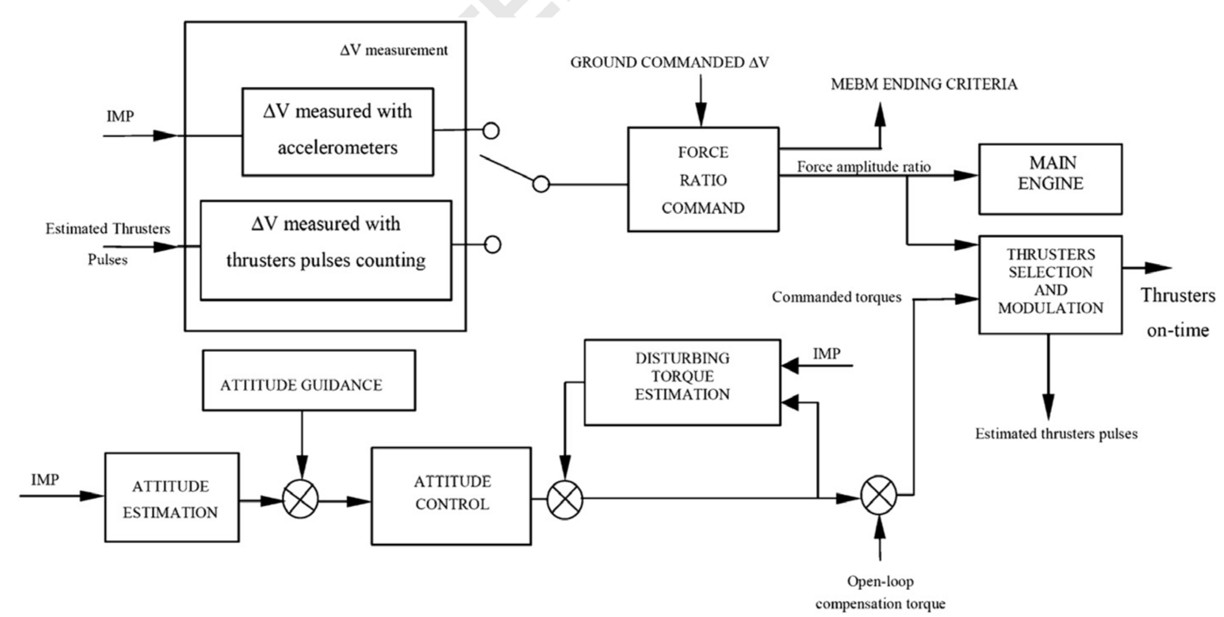

Fig. 4. The attitude and orbit control system.

Identification Procedure

- Satellite state-space model

$$\left.\begin{aligned} \hat{x}_{k+1} &= A\hat{x}_k + Bu_k + Le_k \\ \hat{y}_k &= C\hat{x}_k + e_k \\ e_k &= y_k - \hat{y}_k \end{aligned}\right\}$$

- Identified from simulated data
  - M estimation sequences ($i=1, \ldots, M$)

$$\min_{A,B,C,L} \bar{J} = \min_{A,B,C,L} \sum_{i=1}^{M} J^{(i)}$$

- Estimation of the matrices (A, B, C, L)

$$J^{(i)} = \frac{1}{N} \sum_{k=1}^{N} e_k^2\left(A, B, C, L, \left\{u_k^{(i)}, y_k^{(i)}\right\}\right)$$

Residual Generator Design

- UIO de-coupled from the i-th input ($i=1,\ldots,4$)

$$\begin{aligned} z_{k+1} &= F_{k+1} z_k + T_{k+1} B u_k + K_{k+1} y_k \\ \widehat{x}_{k+1} &= z_{k+1} + H_{k+1} y_{k+1} \\ \hat{y}_{k+1} &= C \widehat{x}_{k+1} \end{aligned}$$

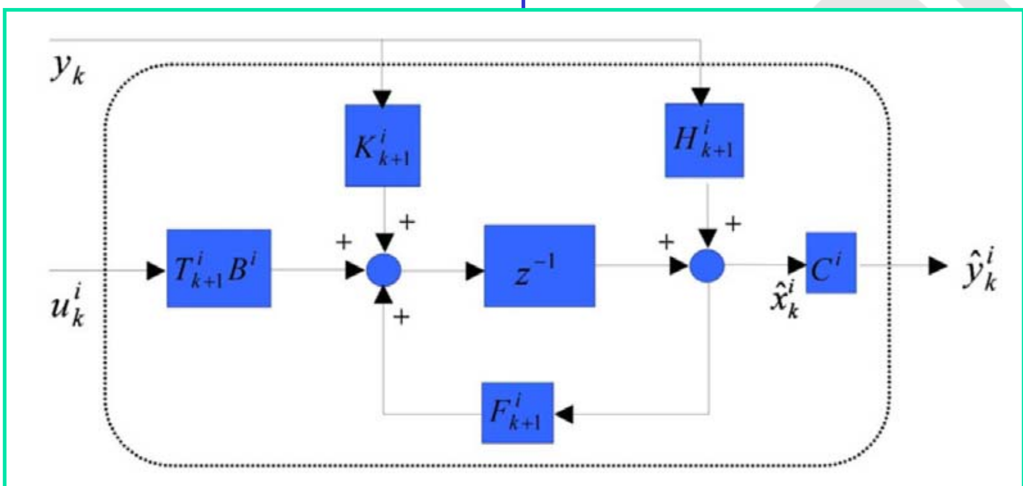

- + 1 observer for the healthy case

Robust FDI

Combination of disturbance estimation and fault de-coupling for robust FDI

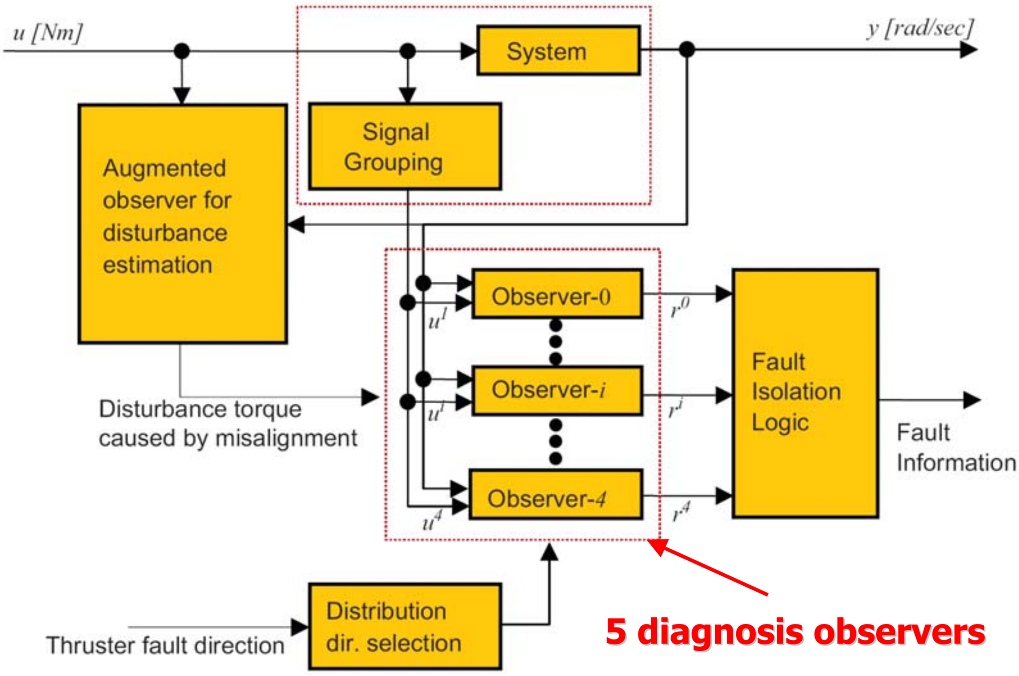

FDI Results

- Residual signals
- Fault detection (from observer $n=0$)
- Fault isolation from UIO$_i$ with smaller residual r_k ($i=1,\ldots,4$)

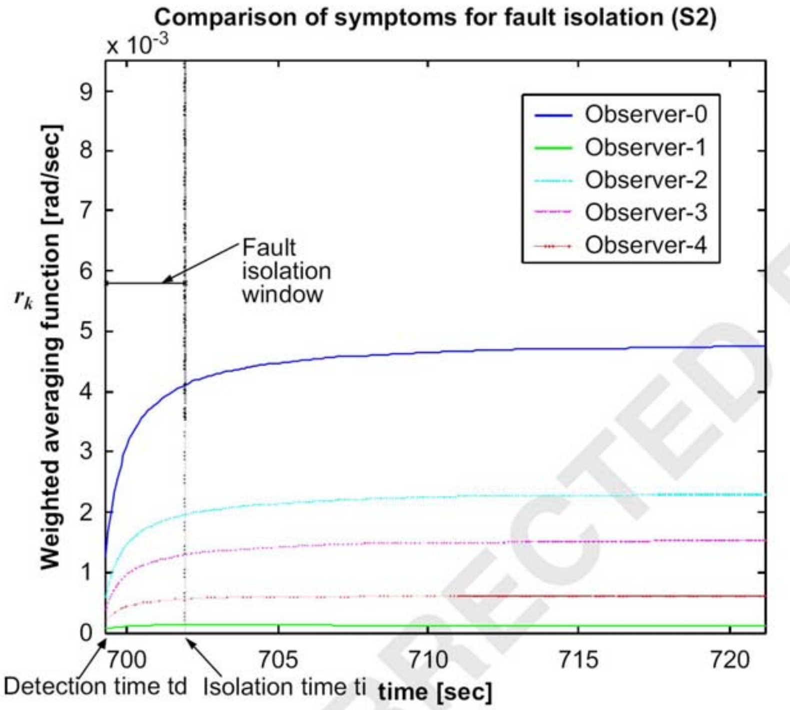

FDI Results (Cont'd)

Fault	r_{fa}	r_{mf}	r_{td}, r_{ti}	τ_{md}, τ_{mi} (s)
Case 1	0.002	0.003	0.997	27
Case 2	0.001	0.001	0.999	18
Case 3	0.002	0.003	0.997	25
Case 4	0.003	0.002	0.998	35

Performance index	Current FDI method	Proposed FDI method
r_{fa}	0.001	0.001
r_{td}	0.999	0.999
r_{ti}	N/A	0.999
r_{mf}	0.001	0.001
Detection time with max de-pointing error (s)	1.08	0.10
Isolation time with max de-pointing error e (s)	N/A	0.11

NOTE:

0.11 rad = 6°

1.08 rad = 61°

Conclusion – Lecture 4

- ✓ Model-Based FDI
- ✓ Analytical Redundancy
- ✓ State-Space Models
- ✓ Residual Generation
  - ✓ Unknown Input Observers UIO
  - ✓ Dynamic Observers / Kalman Filters
  - ✓ Neural Networks and Fuzzy Systems
- ✓ Residual Evaluation/Change Detection
- ✓ Application examples